UNIVERSITY OF CALIFORNIA, SAN DIEGO

Development of Superelastic Effect in Ferrous Shape Memory Alloy

A thesis submitted in partial satisfaction of the requirements for the degree
Master of Science

in

Materials Science and Engineering

by

Scott Olson

Committee in charge:

Professor Kenneth S. Vecchio, Chair
Professor Ying S. Meng
Professor Marc. A. Meyers

2013

The Thesis of Scott Olson is approved and is acceptable in quality and form for publication on microfilm and electronically.

_____

_____

_____
Chair

University of California, San Diego

2013

DEDICATION

In recognition of the guidance he has provided over the past two years, this thesis is dedicated to my advisor, Dr. Kenneth Vecchio.

Additionally, in recognition of all the support they have given me in getting to graduation this thesis is dedicated to my parents, Dr. Doug and Julie Olson.

TABLE OF CONTENTS

LIST OF ABBREVIATIONS

NCATB: Shape memory alloy comprising of iron, nickel, cobalt, aluminum, tantalum, and boron, that is being investigated in this thesis

SMA: Shape memory alloy

SE: Superelastic effect

SME: Shape memory effect

Nitinol: Nickel-titanium shape memory alloy

SIM: Stress-induced martensite

LOM: Light optical microscopy

SEM: Scanning electron microscope

EDS: Energy dispersive spectroscopy

XRD: X-ray diffractometer

HRB: Rockwell B hardness

FCC: Face centered cubic

BCT: Body centered tetragonal

BSE: Back-scatter electron

HRC: Rockwell C hardness

LIST OF FIGURES

LIST OF GRAPHS

LIST OF TABLES

ACKNOWLEDGEMENT

I would like to acknowledge Professor Kenneth S. Vecchio for his support as the chair of my committee, as well as being a very involved advisor the past two years. His guidance has proved invaluable, and taught me many lessons regarding being a professional and well-rounded engineer. I would also like to sincerely thank Steven McCloskey for all of his help in bringing my project to completion.

The introduction, Chapters 1, 2, 3, 4 and Appendix, in part, are currently being prepared for submission for publication of the material. Olson, Scott M.; Vecchio, Kenneth S. The thesis author was the primary investigator and author of this material.

ABSTRACT OF THE THESIS

Development of Superelastic Effect in Ferrous Shape Memory Alloy

by

Scott Olson

Master of Science in Materials Science and Engineering

University of California, San Diego, 2013

Professor Kenneth S. Vecchio, Chair

Shape memory alloys (SMAs) with high levels of superelasticity are used where there is a need for the application of large levels of force, or high damping [1]. Current commercially available SMAs require expensive fabrication and lack sufficient ductility for many applications. There is a need for a superelastic material with better properties and easier processing. Y. Tanaka *et al.* have developed a novel iron based shape

memory alloy, NCATB [2]. This alloy still requires complex thermomechanical processing, and does not utilize lessons learned in optimizing Nitinol.

To develop the properties of this alloy, it was synthesized in lab from its constituent elements, and thermomechanically processed. Samples were prepared for analysis using conventional metallographic techniques, and investigated with light optical microscopy, scanning electron microscopy equipped with energy dispersive spectroscopy, X-ray diffraction, and mechanical testing.

The recrystallization following cold rolling, as well as aging heat treatments, were determined to be critical to increasing the hardness of the NCATB. Overall, smaller grains and longer aging times increased the hardness. The as-cast microstructure exhibits significant tantalum segregation along the dendrite boundaries. Incomplete homogenization of the as-cast microstructure leads to a propensity for a Ta-rich phase to form along subsequent recrystallized grain boundaries. This phase lead to alloy embrittlement, preventing the NCATB as processed from having the desired superelasticity. An additional high temperature thermomechanical treatment following casting solutionized the tantalum from the dendrite boundaries, and further improved the NCATB hardenability.

INTRODUCTION

Interest continues to grow in shape memory alloys, or SMAs, which are defined by their unique shape memory effect, (SME), whereby the material returns to its original cold-deformed structure when heated. This effect fills an important technological void in actuators, pipe joints, medicine, and damping applications by providing large forces and high damping capacity [1]. Associated with the shape memory effect is the superelastic effect, (SE) where the material can undergo high levels of recoverable, elastic strain. In SMAs, the SME and SE are based on the diffusionless, martensitic phase transformation [3]. Martensite is not a phase unique to SMAs; it is well established in steel. However, the martensite that forms in SMAs can be an equilibrium phase or stress induced, and not by necessity formed through a specific heat treatment. Certain steels also exhibit the stress-induced martensite (SIM) called transformation-induced plasticity [10]. Since the martensitic transformation is reversible in SMAs, the original shape can still largely be recovered.

Currently, Nitinol, an alloy made of nickel and titanium in close to equal proportions, is the only commercially available shape memory alloy. It has approximately 7% superelastic strain, but lacks sufficient ductility for most applications and requires expensive fabrication that restricts its use. Ferrous SMAs such as Fe-Mn-Si, Fe-Ni-C and Fe-Ni-Co-Ti exhibit better workability and lower costs, but lack a large degree of superelasticity at room temperature due to poor thermoelastic martensite transformations. These Fe-based SMAs often require costly thermomechanical training to achieve superelasticity, or have embrittlement that prevents them from achieving

superelasticity outside of the single crystal state [2-4]. There has been work done by Cherenko to make the Fe-Co-Ni-Ti SMA thermoelastic by using thermomechanical processing, yielding characteristics similar to the martensitic transformations in NiTi and Cu SMAs [5]. Kajiwara and others have improved the shape memory effect in Fe-Mn-Si alloys by adding Nb and C to form several nanometer, coherent precipitates in the austenite. Similar to NiTi and other SMAs, in this alloy annealing is important to developing the SME [4,11-14,16]. Additionally, rolling before aging has proven essential to increasing the amount of recoverable strain [16]. Maki and others have also found ausaging and the resultant fine Ni_3Ti precipitates necessary to the SME in Fe-Ni-Ti-Co alloys, where longer ausage times hardens the alloy and improves the SME [6]. This ausforming was stated by Kajiwara and Kikuchi to be important as it strengthens the austenite and is an effective way to inhibit plastic deformation, where again more training cycles decreases the martensite plate width, with an increasing number of plates present in the microstructure [7,9]. Crucial in the thermomechanical training of Fe-Mn-Si alloys is creating thin and uniformly distributed, single variant stress-induced martensite plates, which only comes about through the training cycle [4,9].

Another mechanism beyond precipitation hardening found important in SMAs is grain size, as this strengthening influences dislocation slip, and leads to an orientation dependence for the superelastic properties. In most cases, smaller grains enhance the response, although Tanaka and others have reported larger grains improve the superelasticity [2,8,14-15,17]. In essence, the two most important steps in determining the end SE and SME properties in almost all shape memory alloys are cold work and

aging, with increasing levels of work and increasing size and volume fraction of fine precipitates enhancing the end properties [3,18].

Recently, Tanaka *et al.* reported a new ferrous SMA with exceptional superelasticity of 13.5 % recoverable strain and a tensile strength exceeding 1 GPa [2]. These properties are realized when properly processed with fine γ'-$(Ni,Fe,Co)_3(Al,Ta)$ $L1_2$ coherent precipitates on the order of 3 nm, and strong {035}<100> recrystallization texture [2]. This alloy is comprised of Fe-28Ni-17Co-11.5Al-2.5Ta-0.05B (atom percent), abbreviated NCATB for its alloy content. It exhibits a stress-induced martensitic phase transformation, thermoelastic in nature, from its face centered cubic (FCC) γ austenite matrix, with a lattice parameter of a_0 = 0.3604 nm, to a body centered tetragonal (BCT) α' martensite, with reported a = 0.2771 nm and c = 0.3069 nm. The BCT possibly transforms into a body centered cubic (BCC) martensite in the last transformation steps, with a lattice parameter of 0.2867 nm. This would make the stress-induced martensite transformation FCC to BCT and possibly to BCC, upon loading. NCATB reportedly owes its exceptional properties to a careful alloy content choice—where tantalum stabilizes the γ' precipitate and the boron suppresses a detrimental β precipitate from forming on the grain boundaries—as well as to the complex thermomechanical processing it undergoes. As reported, the alloy is cast, hot rolled at 1250°C, γ-solution heat treated at 1300°C for 15 minutes, cold rolled to 98.6 % reduction in thickness, solution treated again at 1300°C for 18 hours, and finally aged at 600°C for 72 hours [2].

Work has been done in developing the single crystal properties of NCATB by

Chumlyakov and others [19-23], where the precipitation of the γ' was found to be critical to the SE properties, although levels of recoverable strain only reached 3.75 % in tension, and 2 % in compression [22]. As these investigations were of single crystals, no boron was added since it was viewed as unnecessary because there would not be grain boundaries. Furthermore, a tantalum carbide was discovered in the alloy, possibly detrimental to the SE and SME. Ma and others put forth a theory regarding the precipitate functionality: since γ' is coherent within the austenite matrix, the stress-induced martensite transformation causes the γ' to distort elastically, storing large amounts of elastic energy at the SIM-precipitate boundary, providing a driving force for the reverse transformation [22]. The SE was also found to be sensitive to the c/a ratio of the martensite, and the martensite variant that formed [22,23]. Clearly, NCATB has some very promising properties, but requires further fundamental research to develop and understand its superelastic and shape memory properties.

This chapter is currently being prepared for submission for publication of the material. Olson, Scott M.; Vecchio, Kenneth S. The thesis author was the primary investigator and author of this material.

CHAPTER 1: MOTIVATION AND OBJECTIVE

From the extensive research that has been performed on NiTi and other shape memory alloys, including ferrous-based SMAs, there is a lot of potential in developing and enhancing the properties of NCATB. Specifically, the importance of cold work and precipitation strengthening is well established in developing the shape memory and superelastic effects. Grain size also has an important role, where by finer grains usually leads to further SE improvement. The current processing reported by Tanaka *et al.* results in large, 400 μm grains in the alloy [2], and work done by Chumlyakov and others on single crystalline NCATB fails to take advantage of cold work in enhancing the SE, attempting to mimic recrystallization texture simply with the single crystal growth direction [19-23]. Both these areas provide motivation for the current work, where the thermomechanical processing, critical to the end superelastic properties for which NCATB is of interest, has not been fully investigated or optimized. There is great potential in refining the processing in a manner that will not only improve the sustainability of this alloy and make it a more viable alternative to NiTi, but also enhance the superelastic properties.

This leads to the objective, where the current work employs lessons learned from the optimization of Nitinol to the thermomechanical processing of this new Fe-based alloy to enable lower processing temperatures, lower mechanical reductions, and ideally enhanced superelastic response.

Objectives:

a) Examine methods to reduce energy required to achieve homogeneity in NCATB alloys.
b) Examine precipitation hardening behavior as a function of temperature between 400°C and 800°C.
c) Examine grain size reduction effect on overall strengthening and superelastic recoverable strain.

This chapter is currently being prepared for submission for publication of the material. Olson, Scott M.; Vecchio, Kenneth S. The thesis author was the primary investigator and author of this material.

CHAPTER 2: EXPERIMENTAL METHOD

Fe-28Ni-17Co-11.5Al-2.5Ta-0.05B (atom percent) was synthesized into a solid, visually uniform alloy from its base elements using an arc melter, and then further homogenized in a large induction melter, both steps in water cooled copper crucibles. The induction melter is equipped with a top copper plate so the sample can be rapidly quenched and forged following the induction step. Hot rolling was performed by heating the NCATB up to 1250°C in a Lindberg box furnace and rolled on a modified mill with forward, reverse, and roll speed controls, where the same mill was used at room temperature for the cold rolling step. Solutionization for 18 hours and all aging heat treatments used a Lindberg tube furnace under inert argon atmosphere, where short-time heat treatments used a Lindberg box furnace in order to have better control over time at temperature.

Initial samples were arc and induction melted to form the homogenous solid, hot rolled to 28 % reduction in thickness, γ solutionized at 1300°C for 15 minutes, cold rolled to varying levels of reduction in thickness, up to the reported 98 %, solutionized again at 1300°C for 18 hours and aged up to 72 hours at 600°C. Samples were taken throughout the process and prepared using conventional metallographic techniques, polished to a diamond finish for XRD and SEM/EDS analysis, as well as etched with Nital (5% nitric acid, 95% methanol) in a submerged bath to reveal microstructural features with the LOM. A Rigaku X-ray diffractometer (rotating anode type and Cu K_α radiation), FEI Quanta 600 SEM equipped with a Brunker Xflash 6160 EDS detector and an Olympus GX51 LOM equipped with Pax-it hardware and software were used.

Material cold rolled to 70 % reduction in thickness, with unchanged initial processing, was γ solutionized at varying times and temperatures to control the resultant grain size, and subsequently aged. Cold rolled samples had first been analyzed using XRD following solutionization at temperatures from 850°C through 1300°C. NCATB with refined solutionization times and temperatures were aged at 600°C with samples taken and hardness measured on a Wilson Instrument's Rockwell B hardness tester, to determine the precipitation hardening behavior of the alloy. Additionally, samples solutionized at 1300°C for 1 minute following 70 % cold-rolled reduction in thickness were aged at 400°C, 500°C, 600°C, 700°C, and 800°C and tested for hardness at increasing time, and analyzed using XRD to determine any precipitate phase variation and its influence on the hardening profile.

Final samples utilized a high temperature thermomechanical heat treatment step in the induction melter following homogenization in order to dissipate grain boundary enrichment in the cast microstructure seen using back-scattered imaging on the SEM, and verified by EDS. The induction melter used a power setting of 78 % through 84 % to melt and homogenize the NCATB, contingent on sample size, where larger samples (45 gram ingots) needed the 84 % power setting, and smaller samples (30 gram ingots) needed the 78 % power setting. Induction heat treatments in the melter of solid-state NCATB ranged from 67 % power to 72 % power, again contingent on sample size. Usually, a power setting of 69 % was appropriate. These samples were then solutionized, cold rolled, recrystallized and then aged. Superelasticity was evaluated using dog-boned tensile samples, 5 cm in length, with an Instron 5982 tensile machine,

following ASTM Standard E8.

Metallographic sample preparation specifically involved mounting samples in Struers Clarofast using Struers specified conditions on a CitoPress-20, with grinding and polishing performed on a Struers Tegramin-20 or a Struers Rotopol-2. On the Tegramin-20, samples were ground with MD Piano papers, 120 grit (6.5 minutes, water, 25N), then 600 grit (4 minutes, water, 20N) and finally 1200 grit (4 minutes, water, 20N). Initial samples were ground on a Struers Rotopol-2 with a Pedemat head, going from 180 grit, to 320 grit, 500 grit, 1200 grit, 2400 grit and finally 4000 grit disposable papers, all for 3 minutes, with the exception of the 180 grit and 320 grit which received 3 minutes each on two papers, for a total of 6 minutes grinding at those steps. All used 25 N force. Polishing was always performed on the Rotopol-2 equipped with a Struers Multidoser, for 7 minutes and 30 N force with 6 micron DiaDuo diamond suspension, 14 minutes with 20 N force using Struers OP-U dosing, and a final water polish for 5 minutes and 20 N force. Etching in the Nital took between 10 and 20 seconds, depending on the sample. These metallographic steps were optimized by trial and error to obtain the best surface finish, without sample pull out or damage in the process, as well as minimal, although unavoidable, SIM formation.

X-ray diffraction was performed from a 2θ of 20° through 120° with a step size of 0.02° and 1 second hold time.

This chapter is currently being prepared for submission for publication of the material. Olson, Scott M.; Vecchio, Kenneth S. The thesis author was the primary investigator and author of this material.

CHAPTER 3: RESULTS AND DISCUSSION

3.1: Hardenability

Hardness testing of the NCATB, throughout the modified processing steps, was used to gauge quickly how the processing steps were influencing the strength of the material. Certainly, hardness and strength are not intrinsically correlated, but it is well established that hardness can be used to estimate strength. Furthermore, strengthening the austenite matrix against dislocation slip and plastic deformation is known to be important in developing the superelastic effect [6-9]. It is reasonable then to use hardness as an indicator of the strength of the austenite matrix, as all hardness tests were performed when the NCATB was in its γ state, with varying degrees of γ' precipitation and grain boundary refinement, but without any artificial polishing-induced or stress-induced martensite. Higher hardness and therefore increased strength in the austenitic matrix should enhance the superelasticity, and therefore is a tool to help evaluate the process refinement.

The Rockwell B hardness scale (HRB) was used with this alloy, as initially the hardness before aging and at shorter aging times was too low for the Rockwell C scale. As hardness values never exceeded the maximum on the HRB scale, it was used exclusively to keep data consistent. However, samples with high hardness were also tested using the Wilson Instrument's hardness tester in ASTM Rockwell C settings, for data completeness.

Before any process refinement could be implemented, the reported processing steps of casting, hot rolling at 1250°C to 28 % reduction in thickness, solutionization at

1300°C for 15 minutes, cold rolling at room temperature to 98 % reduction in thickness, solutionization at 1300°C for 18 hours, and aging at 600°C for 72 hours, were investigated and the microstructural evolution tracked using the combination of XRD and LOM, the results of which can be seen in Appendix A. From these studies, the cold rolling step, second solutionization heat treatment, and aging were areas seen for immediate improvement. Cold rolling to such a high level of reduction in thickness not only limits the scale of useable products to very thin films and foils, but also seemed unnecessary given that it is reported as needing to be so high to maintain strong recrystallization texture, however is followed by an 18 hour heat treatment [2]. Rolling to this level reduction without intermediate annealing also requires a high degree of mechanical work, given the strain hardening that occurs throughout the process. As the subsequent heat treatment is for a long time at a very high temperature, which leads to large grains from extended grain growth, limiting the rolled texture, lower levels of cold rolling could be coupled with more efficient recrystallization to attain the desired texture, but without the high energy expenditure at both steps. Figure 3.1 shows XRD spectrum of cold rolling to 54 %, 68 % and 92 % reduction in thickness. Inlaid with each spectrum are light optical micrographs, where the microstructural features can be seen to be very similar in each condition. Certainly present is a texturing effect, where higher levels of rolling strengthens the α' SIM peaks as well as certain γ and γ' (hkl) values relative to other directions. As the precipitate is believed to be an ordered phase of the FCC matrix, and known to be coherent and compositionally similar, with a 3 to 5 nanometer size uniformly distributed in the austenite, a distinction between the two

phases can only be seen in transmission electron microscopy [2, 22]. However, importantly there is no variation in the peaks present in each spectrum, meaning that all three reductions have the same phases. The SIM forms due to residual strain induced in the polishing process, where the removal of material leads to the thin samples becoming even thinner. Therefore the SIM peak intensities are a function not only of the microstructural refinement, but also of this metallographic step, so cannot quantitatively be analyzed, as larger reductions in thickness means a thinner sample that has had material removed. The presence of the α' in the XRD spectrum does indicate that certain grains are superelastic in nature, a good sign for the end properties of the alloy.

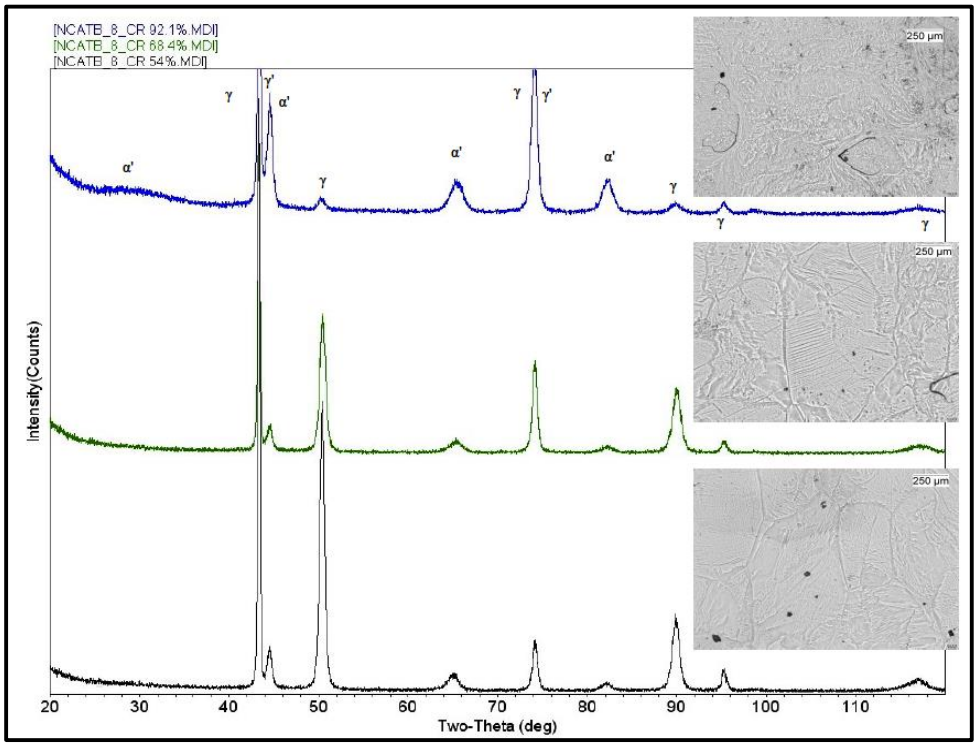

Figure 3.1: XRD spectrum of cold rolled samples at (from bottom to top) 54 %, 68 % and 92 % reduction in thickness, with light optical micrographs inlaid of each step. Note the microstructural similarities at each step, and the same two-theta peaks.

The secondary γ solutionization step is the next processing area seen to have potential for improvement following initial investigations. This step as reported by Tanaka [2] leads to large grains; altering this route could add grain refinement strengthening to the alloy, and ideally enhance the SE response. Finally, a thorough investigation of the aging step was deemed necessary, as work with Nitinol [11] points to its optimization having great importance, given the critical nature of precipitation strengthening in achieving the superelastic response.

3.1.2: Varying the Solutionization Time

Evident from heat treatment investigations at 1300°C following cold rolling is the rapid recrystallization and grain growth of NCATB. Graph 3.1 shows the grain size of 70 % cold rolled samples at increasing times at this solutionization temperature.

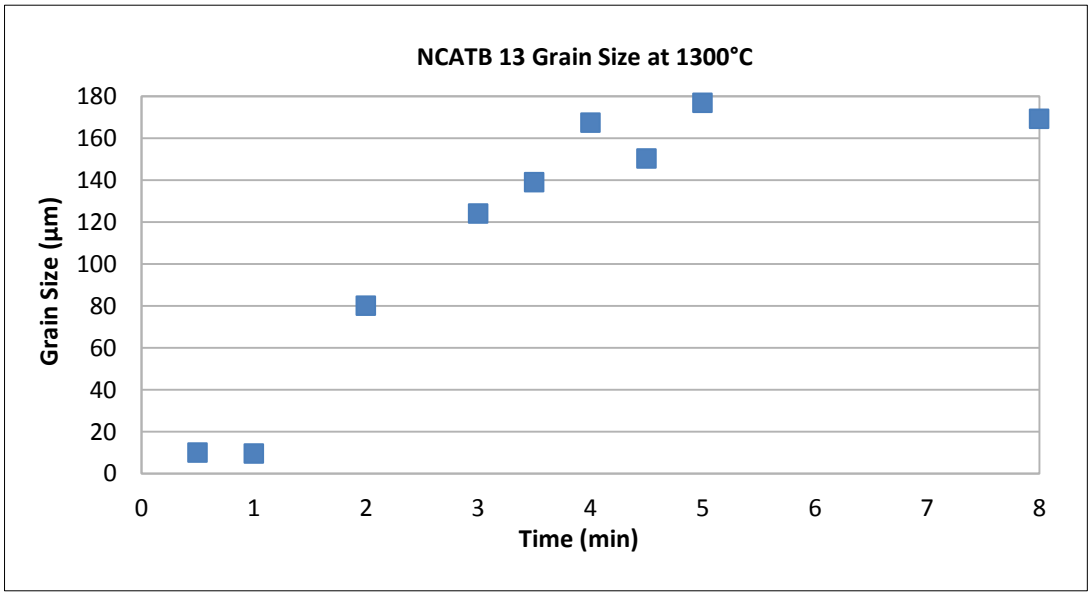

Graph 3.1: Graph showing rapid grain growth that occurs at 1300°C secondary solutionizing heat treatment.

Already by 3 minutes spent at this temperature, the NCATB grains have grown to over 120 µm. The 1 minute and 0.5 minute times have the same average grain size, 10 µm,

but only at 1 minute is the recrystallization complete, and this grain size uniform. To determine if this grain refinement would influence the hardening behavior of NCATB, samples recrystallized at these times were subsequently aged, with HRB values determined throughout the process. Graph 3.2 shows this data, where the finer, uniform grain size achieved by the 1300°C 1 minute heat treatment has the highest hardness throughout the entire 600°C aging process. Certainly, the precipitation hardening predominates and serves as an equalizer, where longer times at 600°C increases the hardness and lessens the effect of the grain size, although it is still present. Graph 3.3 plots the same data as a function of grain size, with an additional series at 400 μm, which is the 18 hour solutionization at 1300°C. The 18 hour solutionization achieves only a 97 HRB hardness, compared to 109 HRB for the 1 minute heat treatment. A 12 point HRB hardness difference is very significant.

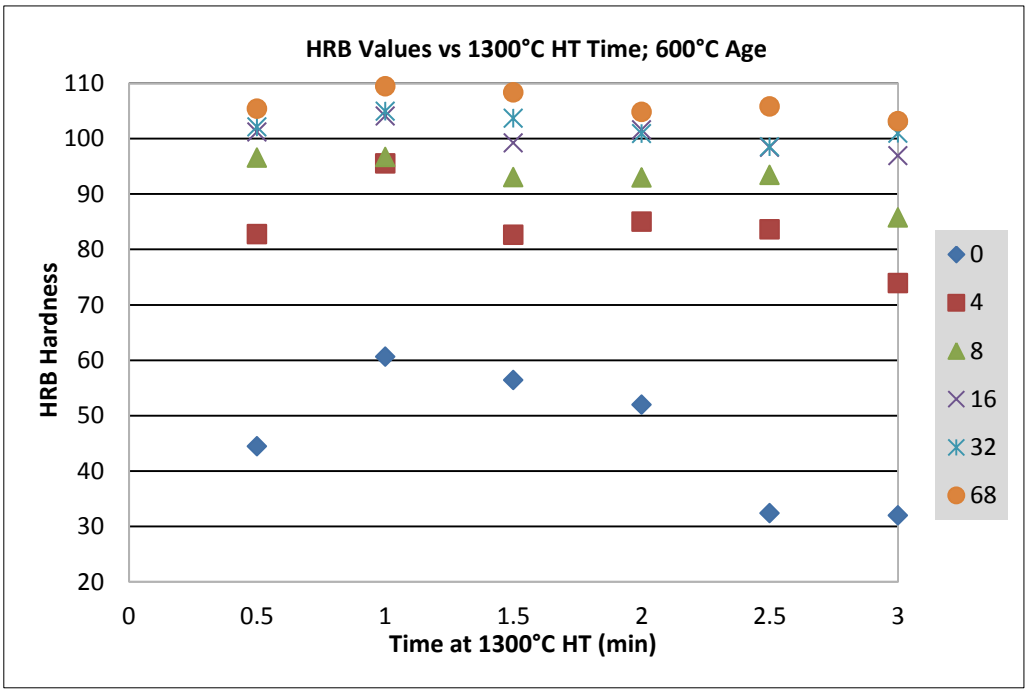

Graph 3.2: Graph showing hardness values as a function of time in secondary solutionization heat treatment at 1300°C. Each series is an aging time (hours).

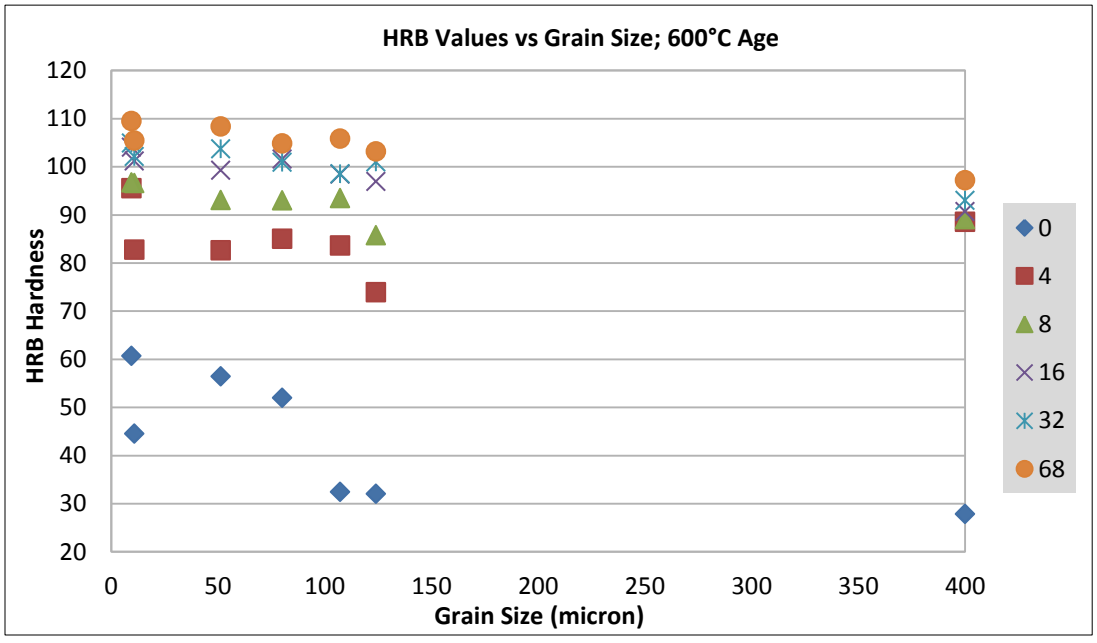

Graph 3.3: Graph illustrating effect of grain size on hardness attained. Note decreasing hardness with increasing grain size, although precipitation hardening serves as equalizer. Each series is an aging time in hours.

3.1.3: Varying the Solutionization Temperature

The stress-induced martensite created in cold rolling is reverted with heat treatments as low as 850°C, seen with XRD. This provides a window for lower energy processing that still achieves martensite-free grains similar to those at 1300°C, entirely comprised of the austenite matrix. Figure 3.2 shows XRD spectrum of cold rolled samples to 91 % reduction in thickness and subsequently heat treated. Even the 600°C heat treatment reverts most of the microstructure back to austenite after just 10 minutes, and at 1000°C the transformation is complete. This data illustrates that lower temperatures may be able to be utilized for broader time ranges to control the grain size. Graph 3.4 demonstrates the grain growth of a sample held at 1225°C, where by 10 minutes the grains are still below 120 μm, the value exceeded with 3 minutes at 1300°C.

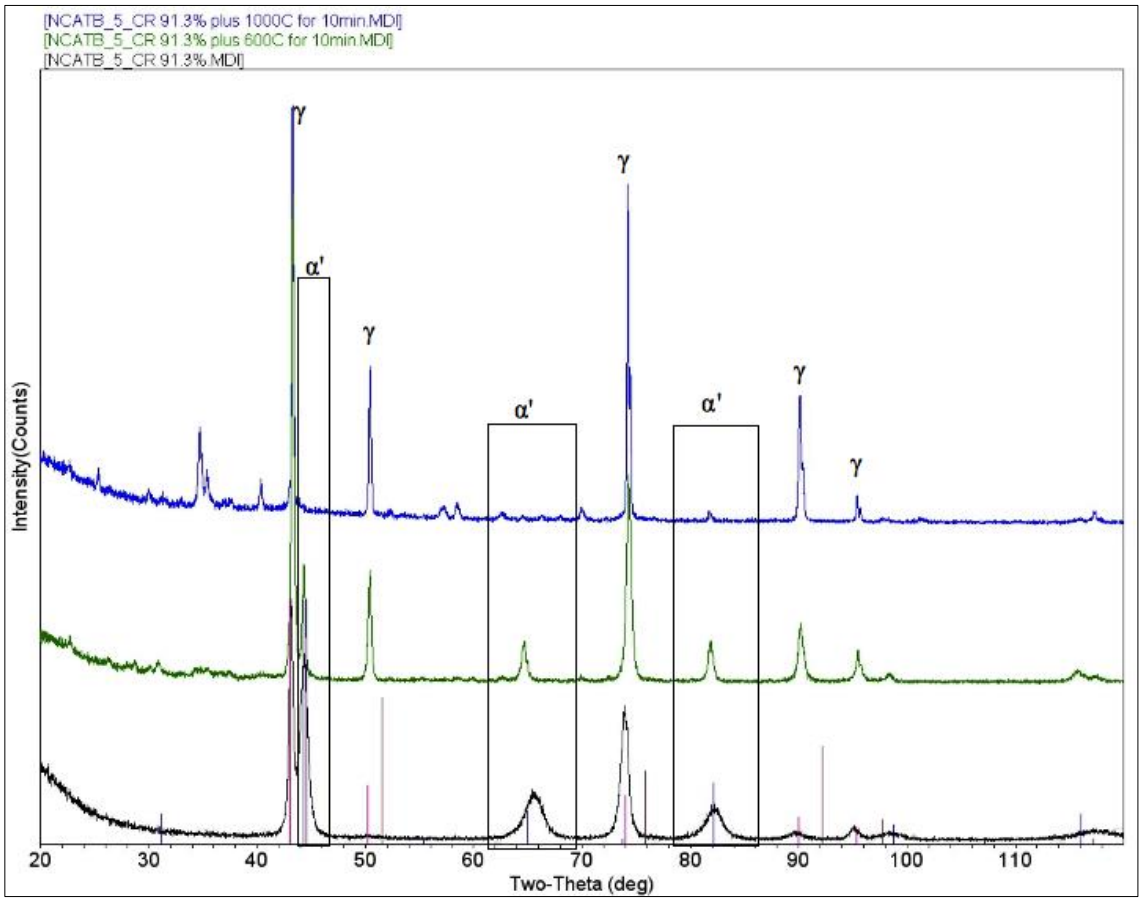

Figure 3.2: XRD spectrum of samples cold rolled to 91 % reduction in thickness and subsequently heat treated for 10 minutes at (from top to bottom) 1000°C, 600°C, and no heat treatment. Note: to preserve SIM integrity, these samples have some residual oxide peaks mostly at $2\theta < 40^{o}$, as SIM can come from oxide removing techniques.

To further strengthen the argument for using lower temperature solutionization, the hardness profile is nearly identical between 1225°C and 1300°C heat treatments with the same resultant grain size, as seen in Graph 3.5.

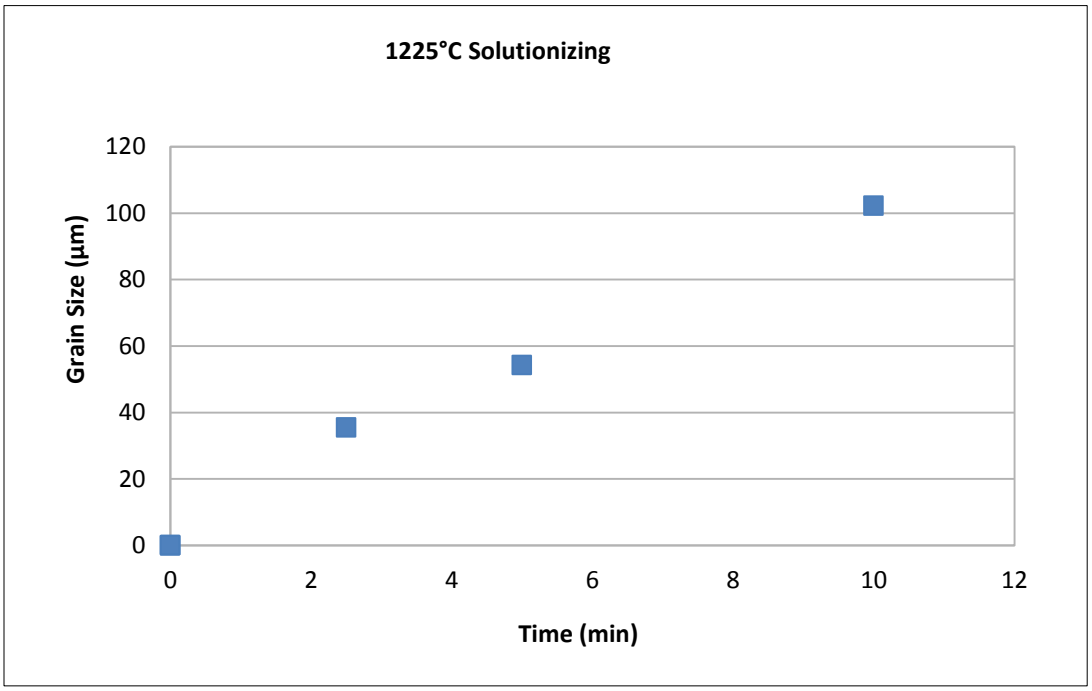

Graph 3.4: Grain size of cold rolled samples subsequently treated at 1225°C.

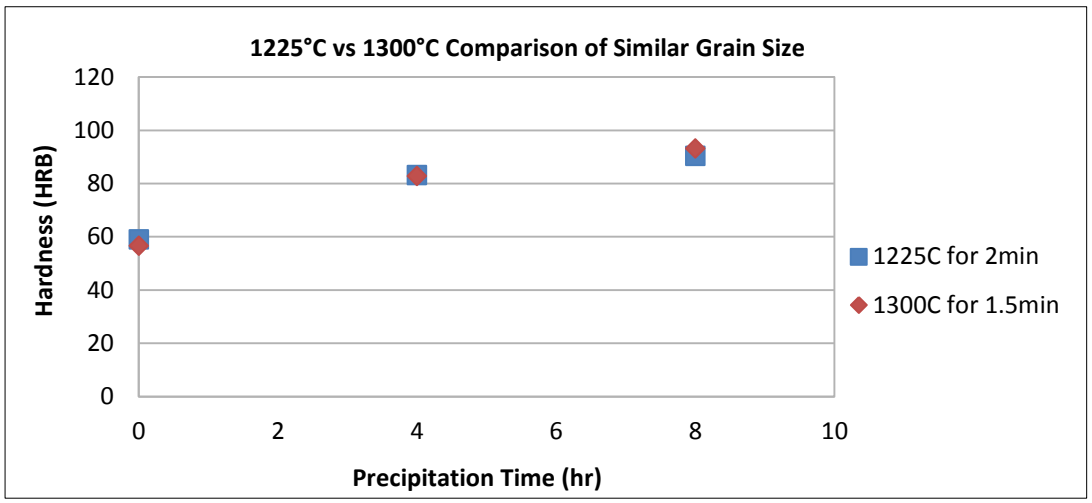

Graph 3.5: Hardening comparison between 1225°C and 1300°C solutionized samples of similar grain size.

Graph 3.6 shows the hardness data through aging for samples solutionized at 1150°C for 12 minutes, 1225°C for 2 minutes, 1300°C for 1 minute, and 1300°C for the full reported 18 hours. As can be seen, initially the hardness values for the lower temperatures are higher, due to some residual cold rolled microstructure that has not fully being reverted to γ as with 1300°C treatments. However, 1300°C still ultimately achieves higher hardness, indicating the strongest austenitic matrix phase.

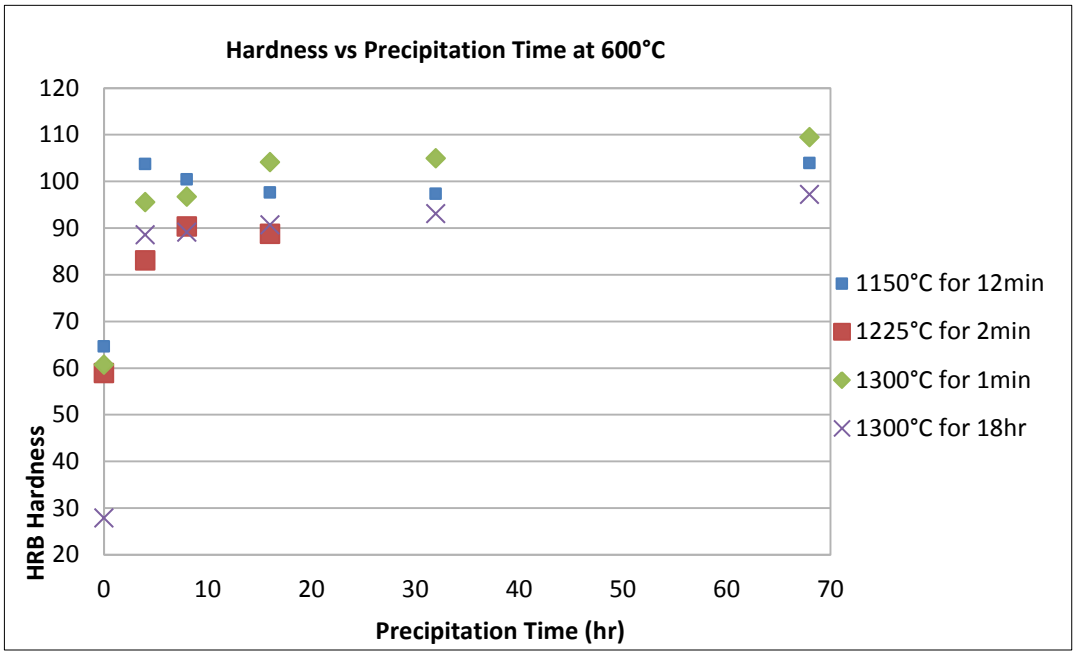

Graph 3.6: Hardening as a function of solutionization temperature.

From these investigations, it is clear that the grain size in NCATB that results from the recrystallization heat treatment following cold rolling influences the hardening behavior, where the small grains achieved through 1300°C for 1 minute are superior to larger grains. It is also apparent that some degree of grain size control, even if not captured at the minimum size, still strengthens the alloy, seen in better hardening through the aging process of the 1.5 through 3 minute 1300°C data compared to 18

hours as reported at this temperature. Apparent as well is that 1300°C is a better temperature choice compared to 1225°C and 1150°C as it ultimately achieves the highest hardness at precipitation times exceeding 16 hours. As previously stated, a strengthened austenite matrix will hopefully resist dislocation slip and plastic deformation, permitting an enhanced superelastic effect by making the SIM favorable, where the stress can be devoted to inducing the phase change of the FCC matrix to the BCT martensite. Nonetheless, the role of precipitation dominates hardening behavior when compared to the grain size effect, motivating research into this processing step, to further strengthen the austenite and improve the SE and SME.

3.1.4: Varying the Precipitation Heat Treatment

Given the reported importance of the γ' precipitate in developing the superelastic properties of NCATB [2,19-24], as well as its determined criticality in the hardening behavior of the alloy, further inquiries into varied temperatures and times at this step were deemed appropriate to evaluate if the austenitic matrix could be strengthened using a better aging path. To this end, samples that had been cold rolled to 70 % reduction in thickness and recrystallized at 1300°C for 1 minute were then aged at 400°C through 800°C in 100°C increments. With an understanding of transformation kinetics, the higher temperature aging samples were removed from the tube furnace at smaller time increments, whereas the lower temperature samples were aged to longer times. The samples were then tested for Rockwell B hardness. Graphs 3.7 and 3.8 display the hardness data on a normal and logarithmic time scale.

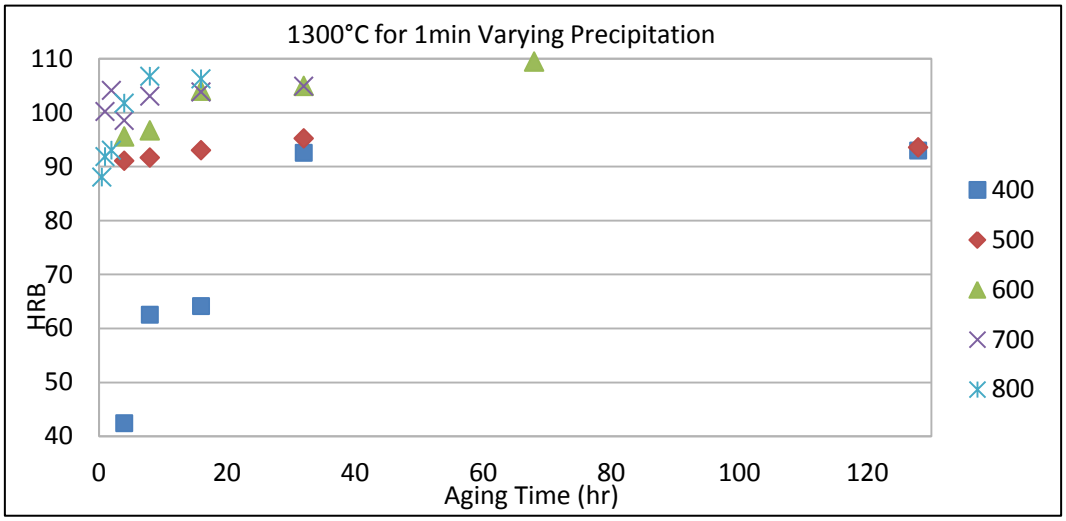

Graph 3.7: Plot of hardness versus aging time for 5 different aging temperature series.

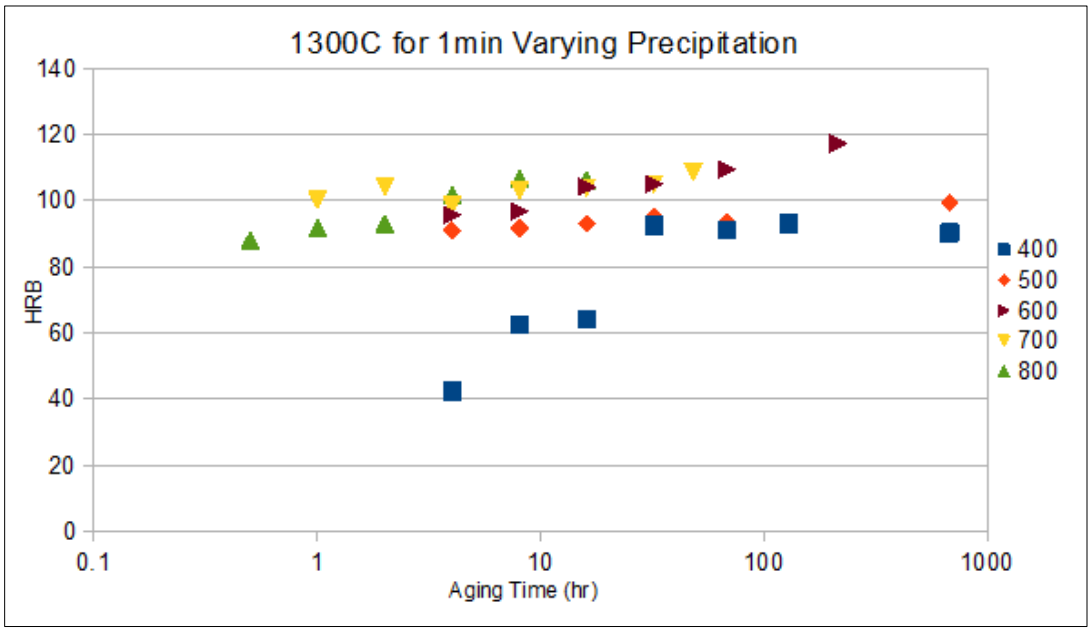

Graph 3.8: Plot of hardness versus logarithmic aging time for 5 different aging temperature series, in Celsius.

Both Graph 3.7 and 3.8 illustrate that the lower temperature aging series of 400°C and 500°C take much longer times to reach comparable hardness values to the 600°C, and even 128 hours aged samples have hardness values of 93 and 94 HRB, respectively. These values are 15 HRB less than the 68 hour 600°C for the equivalent

solutionization, but do have similar hardness to 68 hour aged samples that have been solutionized for 18 hours at 1300°C. Compared to the higher temperature series, the 400°C and 500°C paths take much longer times to harden the γ matrix with the γ' precipitation, and are impractical when other temperatures are available. There is also a drop in the hardness of the 400ºC series, down to 90 HRB at 672 hours, indicating this aging temperature will never harden to as high a level. Should there be some limiting aging temperature condition, these two lower temperatures may yield the desired superelasticity, as they still harden to the same levels of 18 hour solutionized samples as reported by Tanaka [2]. After 28 days, 500ºC samples harden higher to 99 HRB.

The 4 hour aging time, for which all 5 series were sampled, captures the temperature influence on hardness very well, where increasing the temperature at an equivalent time leads to higher hardness. Why the 1 hour and 2 hour 700°C hardness values are greater than that for 800°C aging is not at this time clear. These two values do not seem to trend with the rest of the 700°C aging, as the 4 hour samples at this temperature are lower than the first two hardness values. By 16 hours aged, the 600°C, 700°C and 800°C no longer have significant hardness differences, where they are HRB 104, 104, and 106 respectively. At 32 hours, both the 600°C and 700°C series have HRB values of 105. This is an interesting result in that the initial dependence on aging temperature has been somewhat eliminated at relatively low aging times, perhaps indicating that the route to achieving the γ' precipitation is less important than its coherence, dispersive nature, and volume fraction. It is possible that 400°C and 500°C do not achieve these qualities with the precipitate, therefore at 128 hours only harden to

levels equivalent to 4 hours at 600°C, with the hardness drop at 672 hours in the 400°C series. However, there remained the possibility that the different aging temperatures would result in different precipitates being formed, with basis in Nitinol being demonstrated by Adharapurapu [11]. Figures 3.3 through 3.6 reveal from XRD that no new phases are developed at these varied aging temperatures, just the expected FCC austenitic γ matrix with embedded ordered $L1_2$ γ' precipitates, and the α' BCT stress-induced martensite. Coupled with the hardness data, the XRD data points to the 700°C and 800°C series having superelastic potential at reduced aging times.

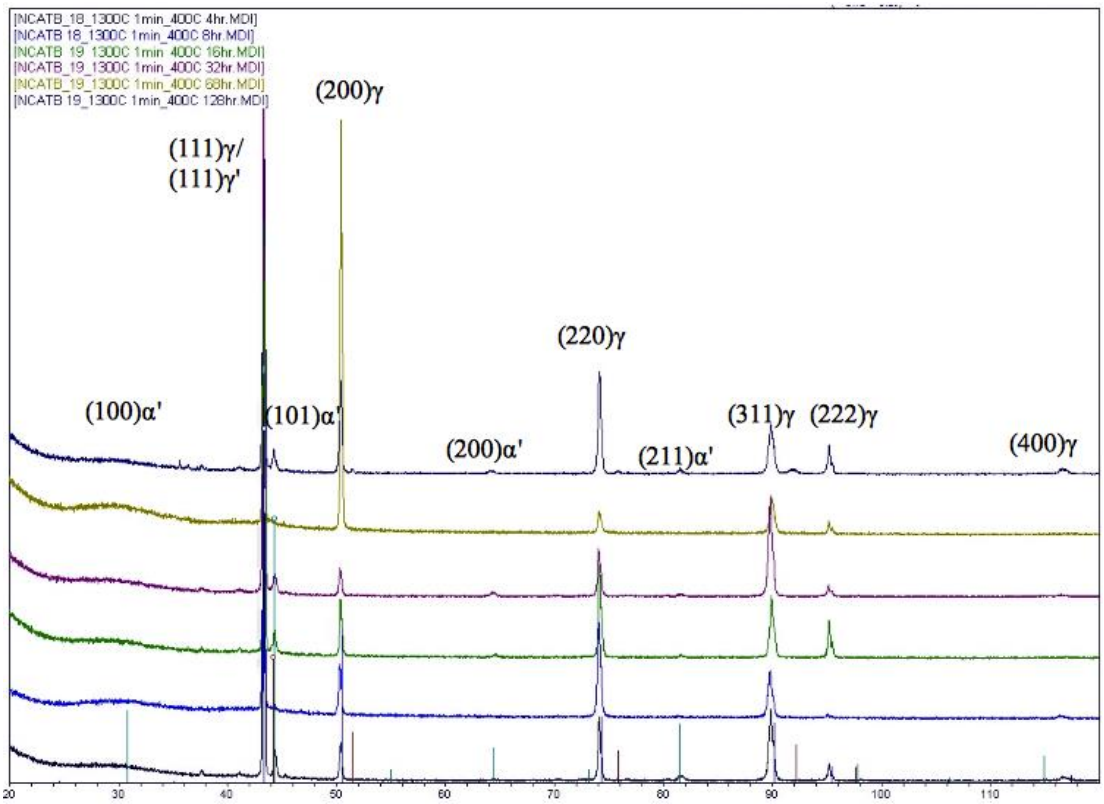

Figure 3.3: XRD spectrum of 400°C aging times at (from bottom to top) 4, 8, 16, 32, 68 and 128 hours.

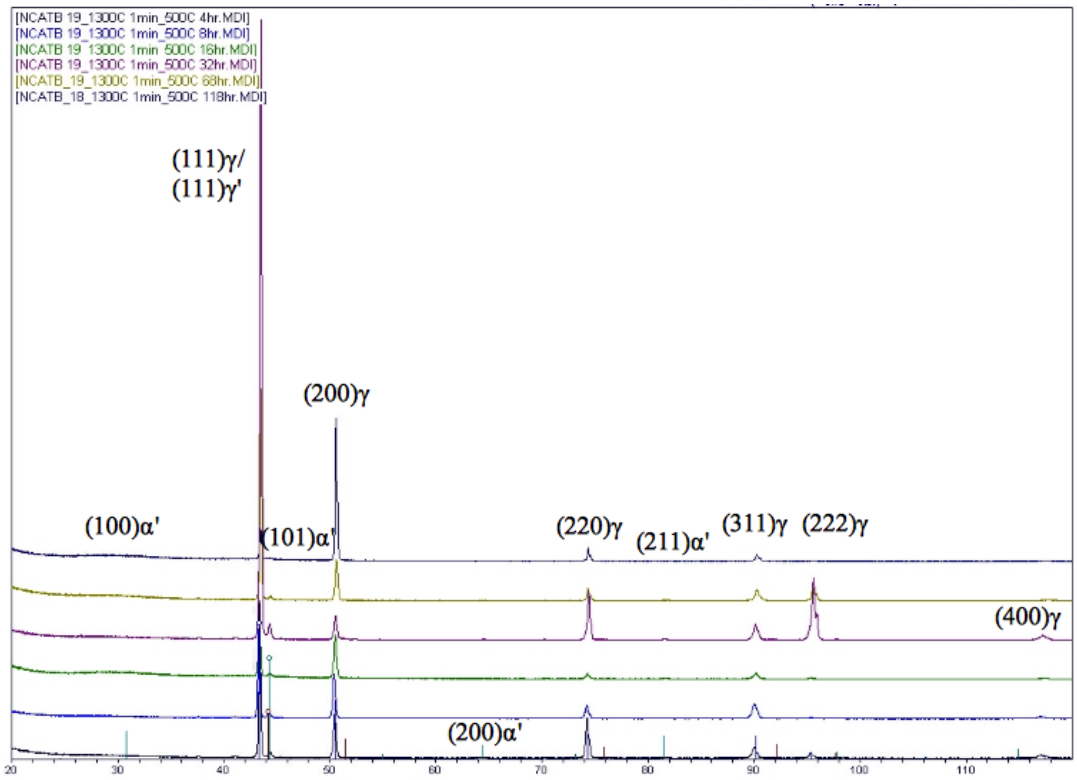

Figure 3.4: XRD spectrum of 500°C aging times at (from bottom to top) 4, 8, 16, 32, 68 and 128 hours.

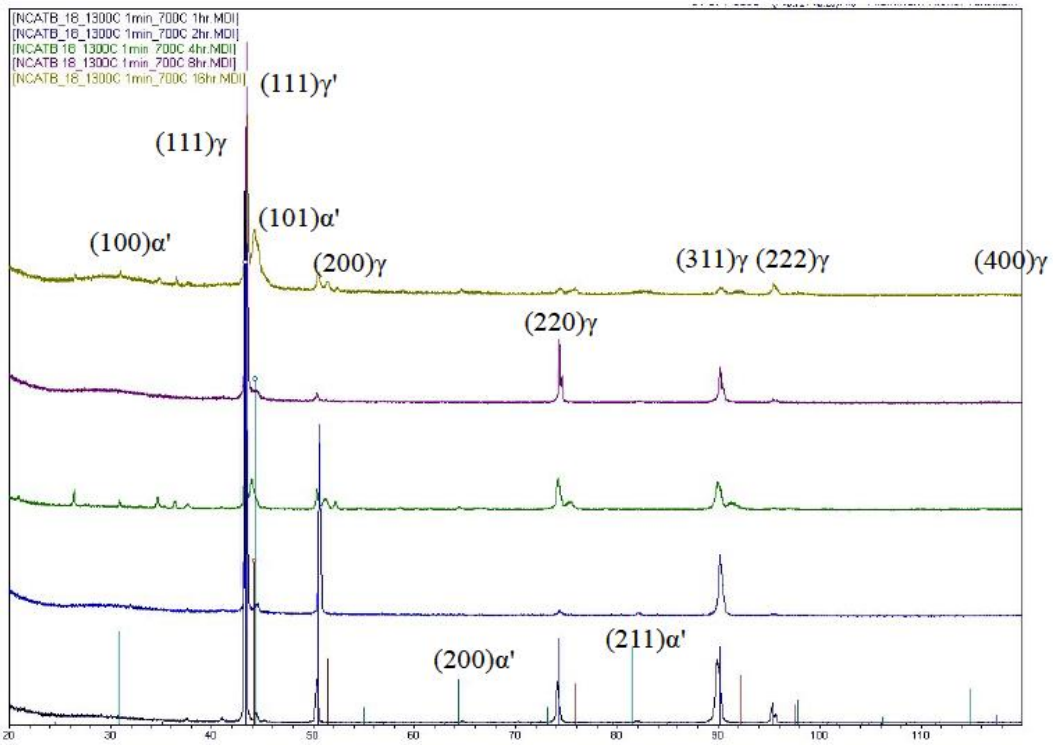

Figure 3.5: XRD spectrum of 700°C aging times at (from bottom to top) 1, 2, 4, 8, and 16 hours.

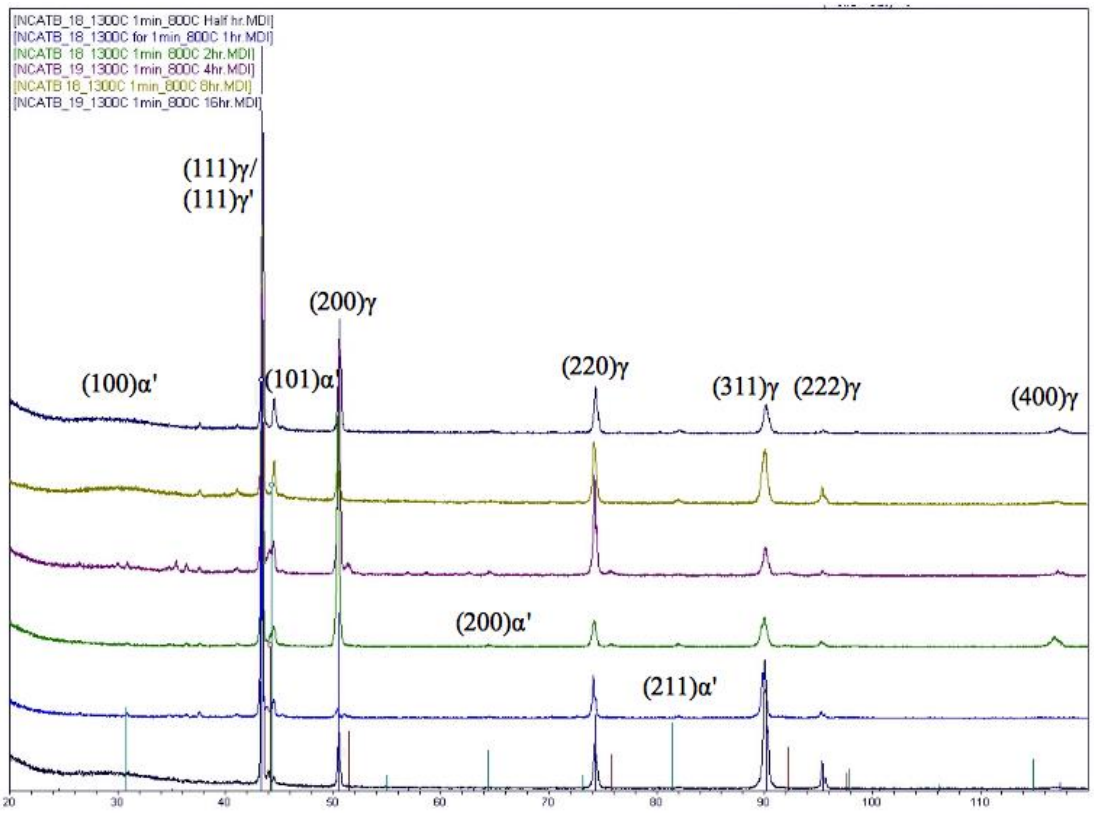

Figure 3.6: XRD spectrum of 800°C aging times at (from bottom to top) 0.5, 1, 2, 4, 8, and 16 hours.

Seen in Graph 3.8, a sample was aged at 600°C for 213 hours, with further hardening up to HRB 117, or Rockwell C 54 when tested on this scale. Figure 3.7 reveals its microstructure from XRD. Importantly, there are no new phases formed, but as the alloy substantially hardened over the 68 hour aging time, precipitate saturation was likely not yet achieved. Longer aging times may be a method for further improving the superelastic effect. Certainly, 213 hours or nearly 9 days, is a long aging treatment, but the NCATB has 7 % hardness improvement over the 68 hour aging time, likely a substantial strengthening of the austenitic matrix. The influence of this hardened γ due to the γ' precipitation on the austenite's resistance to dislocation motion and plastic deformation, allowing for the stress-induced martensitic transformation, needs to be

determined. Certainly, it should make the SIM more favorable by inhibiting the plasticity of the matrix.

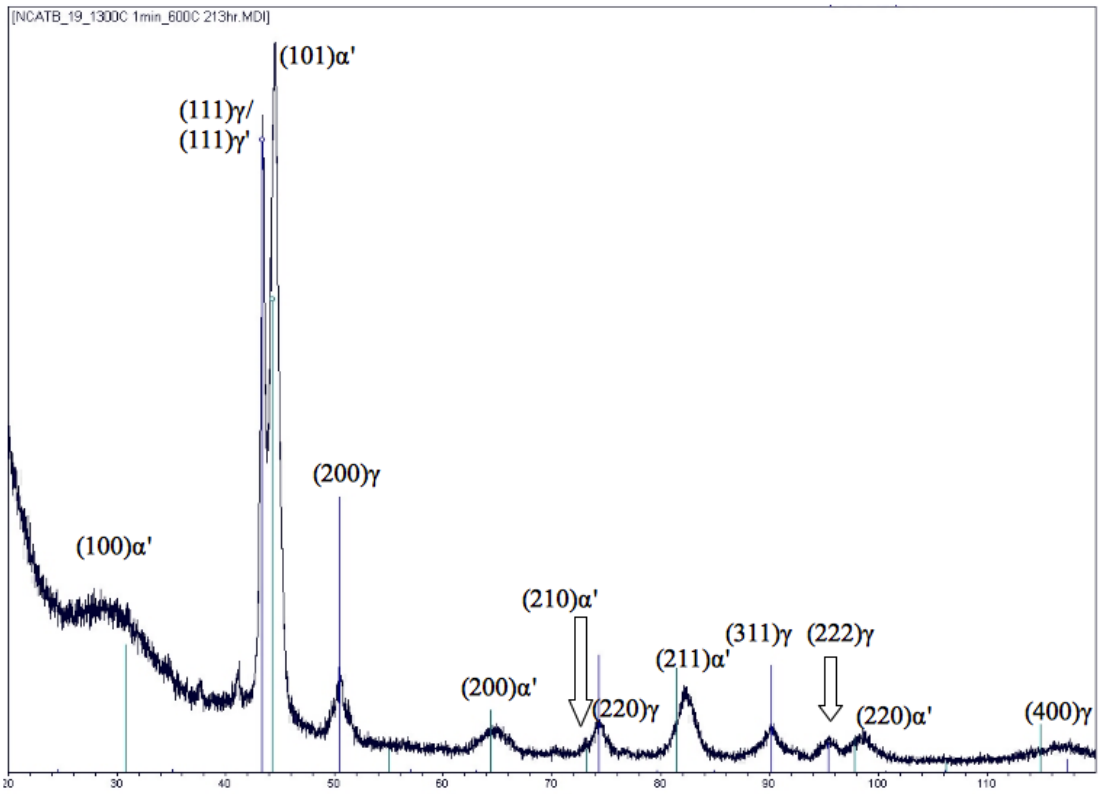

Figure 3.7: XRD spectrum of 1300°C for 1 minute solutionized sample aged to 213 hours at 600°C.

Comparing Figure 3.7 to Figures 3.3 through 3.6, the 213 hour aged sample has broader, less defined peaks. This is more similar to samples aged following the 1300°C for 18 hour solutionization post cold rolling, seen in Figure 3.8. As with all aged samples that were solutionized for 1300°C for 1 minute, there is a texturing effect regarding the (hkl) peaks present, and their relative intensity, indicating differences in the microstructure depending on the solutionization. The results of this difference follow in the next section.

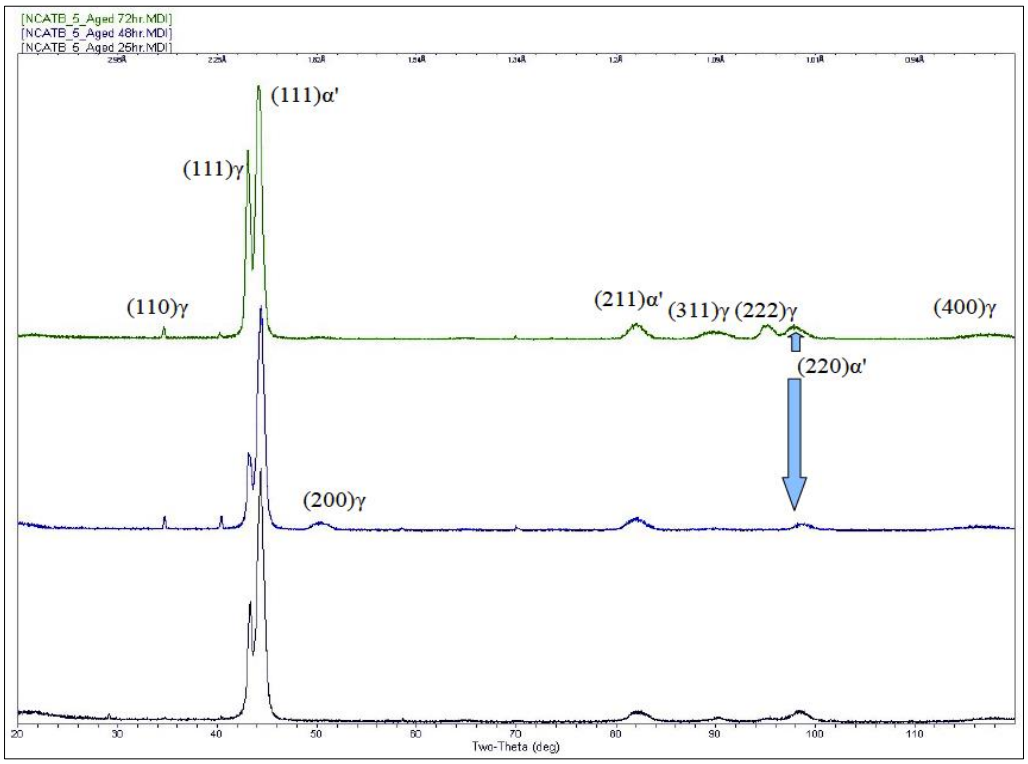

Figure 3.8: XRD spectrum of (from bottom to top) 25, 48 and 72 hour aged samples at 600°C following 1300°C for 18 hour solutionization.

3.2: Superelastic Development

Although the hardening investigations established better processing paths that utilized grain refinement strengthening with similar solutionization temperatures at only fractions of the reported time, the discrepancies between the aged XRD spectrums for the 18 hour and 1 minute solutionization caused concern in achieving superelastic behavior. Indeed, both paths lead to stress-induced martensite being developed in the polishing metallographic preparation step, seen with XRD and optically. Figure 3.9 is a typical micrograph taken of the fully solutionized and aged material, with the martensite plates clearly visible in the grains. The SIM is seen optically as well in all samples that show the α' peaks in the XRD spectrum.

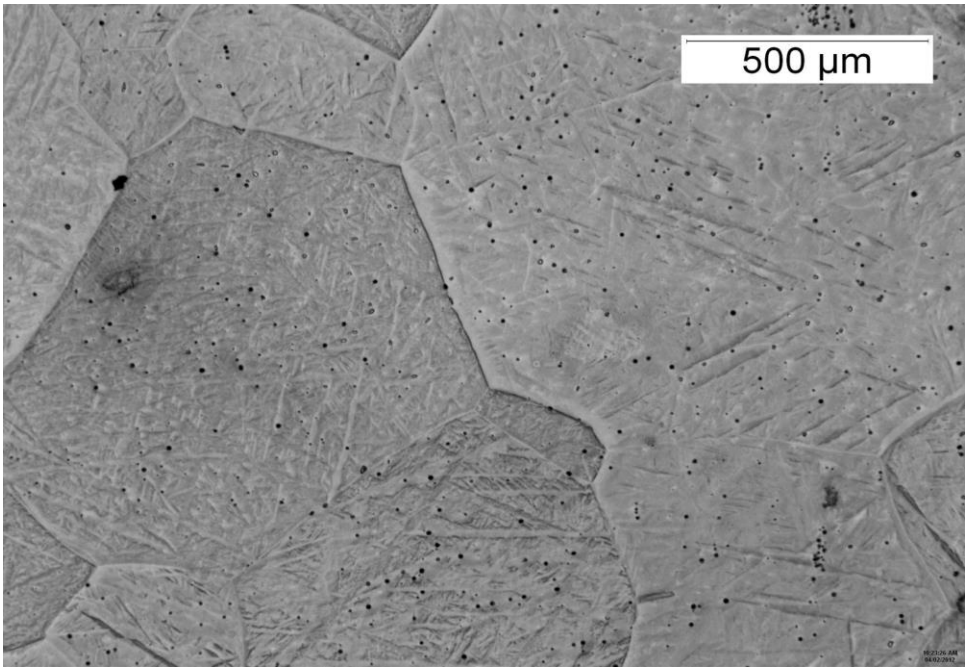

Figure 3.9: Typical micrograph of fully aged NCATB, polished to diamond finish. Note this sample has followed reported 1300°C for 18 hours and 72 hours at 600°C.

The presence of the SIM in LOM and XRD analysis is a definitive indicator that the grains themselves achieve superelasticity. However, the NCATB had embrittlement problems. Tanaka *et al.* report that boron is necessary to prevent the β precipitates from forming on grain boundaries and embrittling the alloy [2]. The current work found that the first 1300°C for 15 minute solutionization that precedes cold rolling, when performed in a box furnace in an air atmosphere, caused a high degree of oxidation detrimental to the alloy. The loss of ductility prevented cold rolling, with edge cracks developing and propagating through the width, causing failure. To overcome this problem, a simple steel box around the sample, to serve as an oxidation barrier, was sufficient to allow for full cold rolling. Enough oxidation remained causing the oxide to be rolled into the sample, found in preparation attempts for transmission electron microscopy. Therefore, the NCATB oxide was mechanically removed following the 15 minute solutionization before cold rolling, and the oxide-free NCATB base metal rolled easily. The samples that were mechanically returned to the base metal were thought to have had the embrittlement problem solved. Full NCATB aged plates having over 1 mm thickness still fractured during flattening for machining and in cutting into tensile specimens. This is very problematic because regardless of what superelastic properties the individual grains possess, a sample that cannot be loaded cannot exhibit superelasticity. Indeed, optical micrographs revealed a grain boundary phase still present in aged samples, seen in Figure 3.10. This is not the coherent γ' precipitate, which is far too small to be viewed optically.

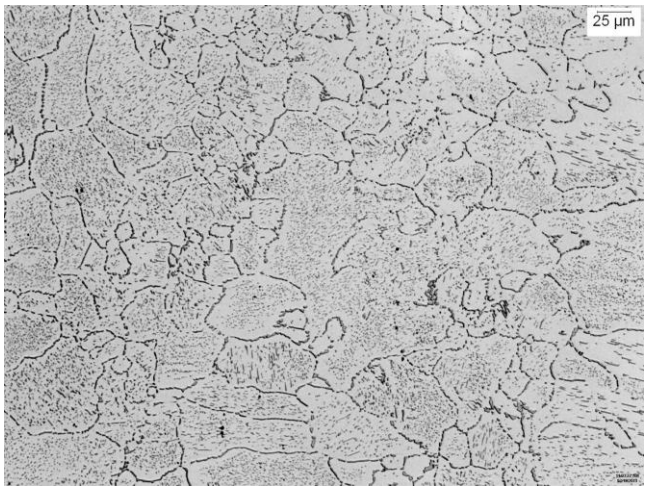

Figure 3.10: LOM micrograph of sample exhibiting grain boundary phase suspected of embrittling alloy. 1150°C for 12 minute solutionization and 4 hour 600°C age.

Certainly the presence of this phase needs eliminating, but the exceptional hardenability as well as the fact that the phase did not show up in XRD analysis indicated that this phase is still of the same FCC γ structure. Therefore, further process refinement could hopefully eliminate this phase and the embrittlement with it, maximizing the superelastic potential of NCATB.

3.2.2: Dendrite Enrichment

Although secondary electron imaging on the SEM did not reveal a phase difference between the matrix and grain boundary phase, back-scatter imaging did. Figure 3.11 shows a BSE image of a 1300°C for 1 minute solutionized sample with the grain boundary phase seen clearly in white. This image can be compared to Figure 3.12, which is of an 18 hour solutionized sample, where this phase has been eliminated. This indicates that the long time reported and employed for the solutionization following cold rolling is necessary to fully homogenize the alloy after casting segregation, and to prevent the embrittlement of the alloy resulting from pushing this segregation to the

grain boundary. Tied to this heat treatment is the 98.6 % cold rolled reduction in thickness needed at such a high level to maintain strong recrystallization texture, as the 18 hours at 1300°C likely eliminates any texturing at rolling levels as low as 90 %, reported by Tanaka *et al.* [2]. If this grain boundary phase could be eliminated by processing steps prior to the secondary solutionization following cold rolling, grain boundary refinement could be utilized to enhance the superelasticity of NCATB at lower cold-rolled reductions in thickness.

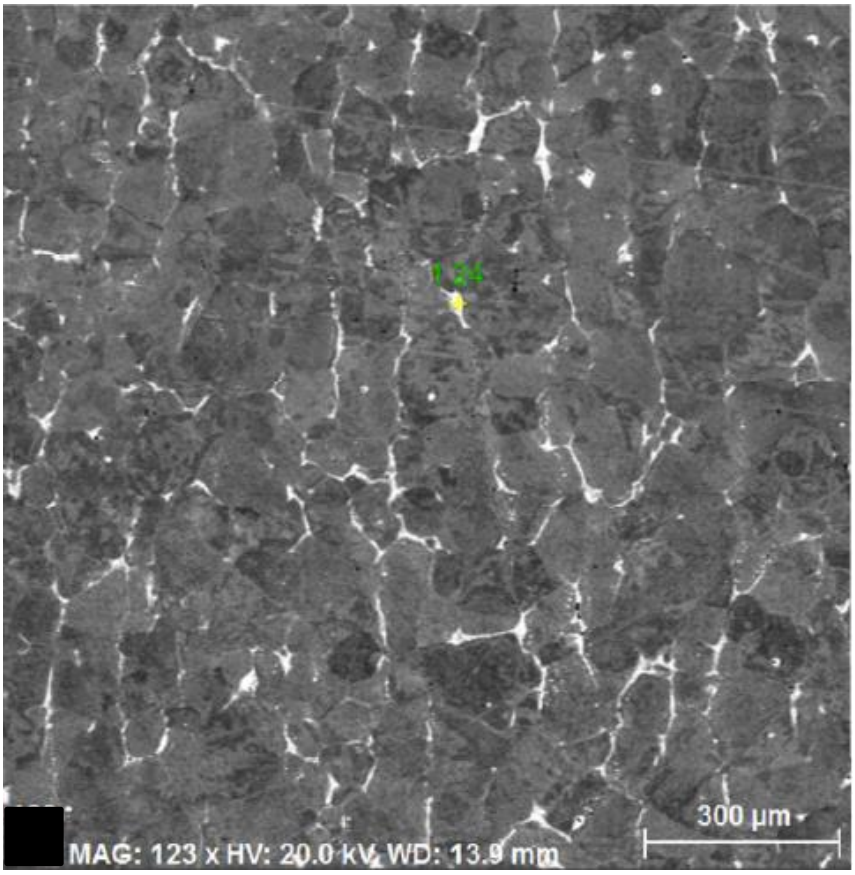

Figure 3.11: BSE image of un-aged 1300°C for 1 minute sample.

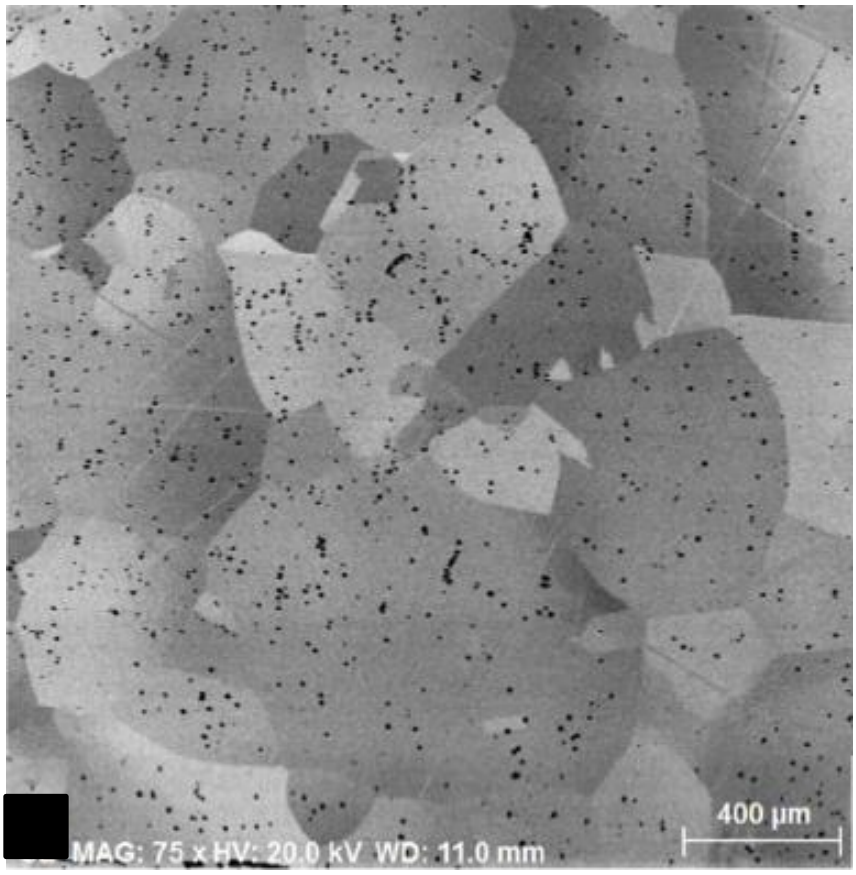

Figure 3.12: BSE image of un-aged 1300°C for 18 hours sample.

Table 3.1: EDS analysis of grain boundary phase in 1300°C for 1 minute un-aged sample. Note higher levels of Ta (at%), normally 2.5 at%

El	AN	Series	unn. C [wt.%]	norm. C [wt.%]	Atom. C [at.%]	Error (1 Sigma) [wt.%]
Fe	26	K-series	35.42	38.45	39.69	0.98
Ni	28	K-series	26.49	28.75	28.24	0.75
Co	27	K-series	16.54	17.95	17.56	0.48
Al	13	K-series	4.96	5.38	11.49	0.28
Ta	73	L-series	8.72	9.47	3.02	0.30
		Total:	92.12	100.00	100.00	

Table 3.2: EDS analysis of grain boundary phase in 1300°C for 1 minute un-aged sample. Note higher levels of Ta and Al (at%), normally 2.5 and 11.5 at% respectively

El	AN	Series	unn. C [wt.%]	norm. C [wt.%]	Atom. C [at.%]	Error (1 Sigma) [wt.%]
Ni	28	K-series	29.70	31.14	31.54	0.84
Fe	26	K-series	24.42	25.61	27.26	0.69
Al	13	K-series	8.14	8.54	18.81	0.43
Co	27	K-series	15.41	16.16	16.30	0.45
Ta	73	L-series	17.70	18.56	6.10	0.55
		Total:	95.37	100.00	100.00	

EDS analysis on the grain boundary phase revealed with BSE imaging is determined to be tantalum and sometimes aluminum rich, coming mainly at the cost of iron, seen in Tables 3.1 and 3.2, of two locations. Iron, nickel and cobalt have sequential atomic numbers, and tantalum is a large, slow atom relative to these other elements. It is almost certain that this grain boundary phase is formed in the casting process, due to tantalum being pushed to the solid-liquid interface in solidification. If this is the case, the segregate should also be present in the as cast dendritic microstructure resulting from the arc and induction melting. Ma *et al.* [22] also report a tantalum carbide phase in the NCATB following their single crystal growth of the material. Figure 3.13 shows a BSE image of NCATB cast from arc melting that confirms the solidification segregation assessment, with Table 3.3 showing a typical compositional make up of this phase using EDS.

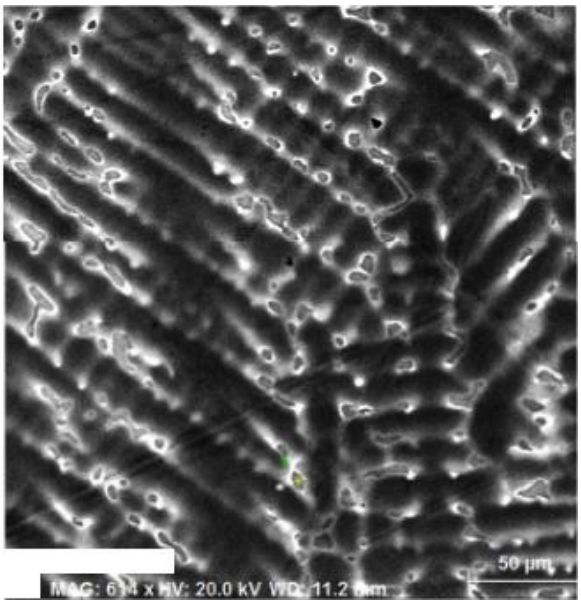

Figure 3.13: BSE image of as cast dendritic microstructure following arc melting. White phase at dendrite boundaries is Ta and Al enriched.

Table 3.3: EDS analysis of dendrite boundary phase in arc melting cast sample.

El	AN	Series	unn. C [wt.%]	norm. C [wt.%]	Atom. C [at.%]	Error (1 Sigma) [wt.%]
Ni	28	K-series	28.22	30.68	29.60	0.80
Fe	26	K-series	26.20	28.48	28.88	0.73
Al	13	K-series	9.33	10.14	21.28	0.49
Co	27	K-series	15.10	16.41	15.77	0.44
Ta	73	L-series	13.15	14.29	4.47	0.42
		Total:	91.99	100.00	100.00	

The tantalum and aluminum segregation is also present in the cast microstructure that follows the induction melting homogenization, seen in Figure 3.14 with a typical composition displayed in Table 3.4.

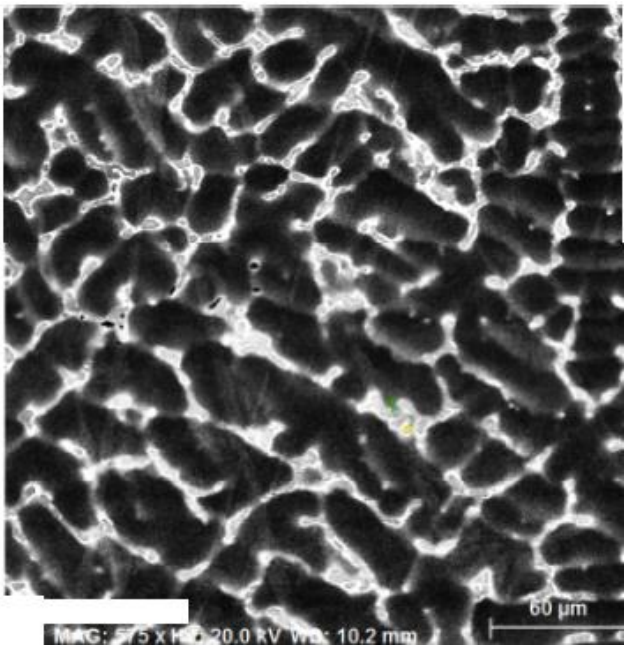

Figure 3.14: BSE image of as cast dendritic microstructure following induction melting. White phase at dendrite boundaries is Ta and Al enriched.

Table 3.4: EDS analysis of dendrite boundary phase in induction melting cast sample.

El	AN	Series	unn. C [wt.%]	norm. C [wt.%]	Atom. C [at.%]	Error (1 Sigma) [wt.%]
Fe	26	K-series	27.58	30.85	31.47	0.77
Ni	28	K-series	27.26	30.49	29.59	0.77
Al	13	K-series	8.06	9.02	19.04	0.43
Co	27	K-series	14.50	16.22	15.68	0.43
Ta	73	L-series	11.99	13.41	4.22	0.39
		Total:	89.38	100.00	100.00	

As the solidification is responsible for causing the tantalum and in some cases aluminum segregation, elimination of this enrichment immediately would allow for the full employment of lessons learned in the optimization of Nitinol and other SMAs, since the NCATB is not re-melted after the induction melting step.

3.2.3: Process Improvement

To eliminate the tantalum segregation in the dendritic microstructure, a high temperature heat treatment was employed in the induction melter immediately

following the induction liquid-homogenization. The NCATB was formed into a solid from its base elements in the arc melter, flipped and melted four times, transferred to the induction melter, re-melted to homogenize the NCATB and rapidly cooled between the copper plates with induction forging. All steps were performed in an inert argon atmosphere first purified by pumping to vacuum, purging the chamber with argon, and repeating three times. Following the induction homogenization step, a new high temperature heat treatment step was added in the induction melter, where the sample was heated for 10 minutes at the highest power setting that the NCATB was still solid. This heat treatment dissipated the tantalum enrichment in the middle of the sample, which gets hotter than the edges, as seen in the BSE image in Figure 3.15, where there is no white phase present. The segregation was also reduced at the edges, seen in Figure 3.16, with the composition from EDS in Table 3.5.

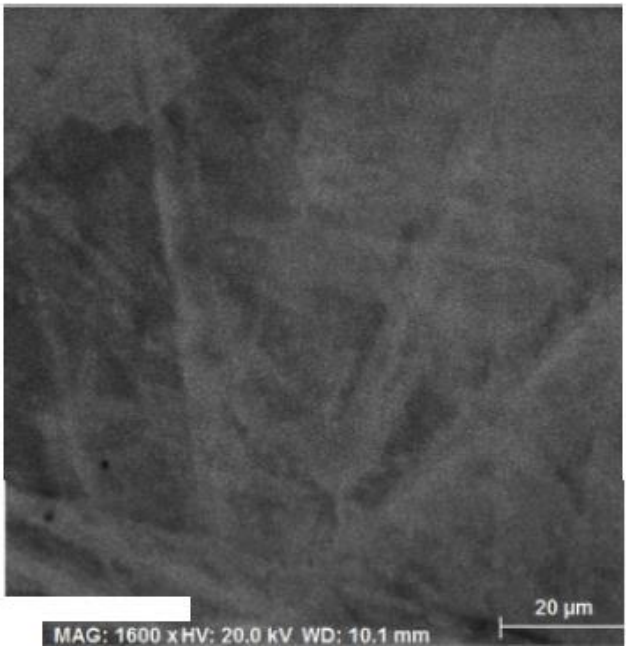

Figure 3.15: BSE image of bulk of sample induction heat treated for 10 minutes.

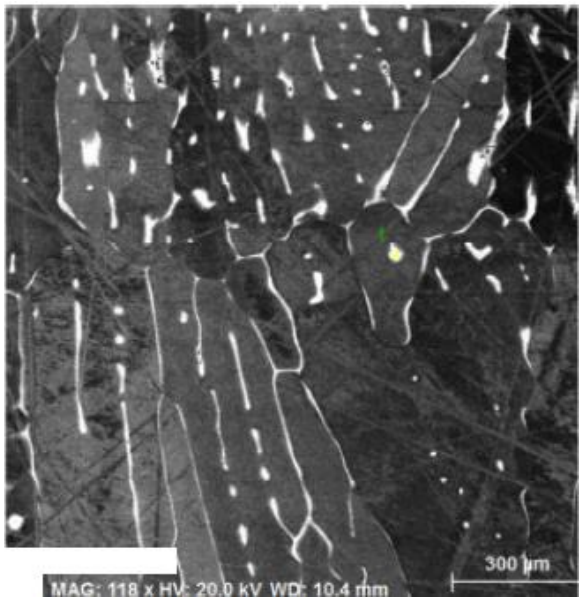

Figure 3.16: BSE image near surface of sample induction heat treated for 10 minutes.

Table 3.5: EDS analysis of boundary phase near surface of sample induction heat treated for 10 minutes.

El	AN	Series	unn. C [wt.%]	norm. C [wt.%]	Atom. C [at.%]	Error (1 Sigma) [wt.%]
Fe	26	K-series	22.86	25.04	29.92	0.65
Ni	28	K-series	22.71	24.88	28.28	0.65
Co	27	K-series	13.55	14.84	16.80	0.40
Al	13	K-series	5.21	5.71	14.12	0.29
Ta	73	L-series	26.95	29.52	10.88	0.80
		Total:	91.29	100.00	100.00	

Another 10 minutes was added at this power setting in the induction melter, to hopefully completely dissipate the enriched boundary phase. However, as can be seen in Figure 3.17, the enrichment has not yet been solutionized.

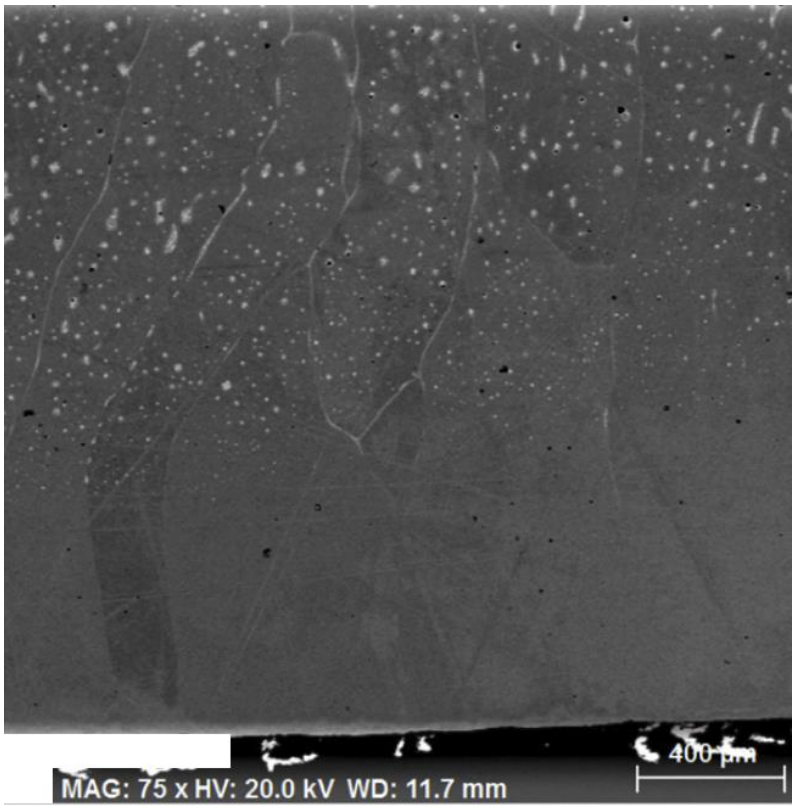

Figure 3.17: BSE image of NCATB with 20 minute induction heat treatment.

Although again the additional high temperature heat treatment disperses more of the tantalum segregation, it is not yet complete. Therefore, one sample was cold rolled to 20% reduction in thickness to mechanically disperse the tantalum, and subsequently induction heat treated for an additional 10 minutes (Figure 3.18) and 20 minutes (Figure 3.19). The rolling step markedly improved this problem, compared to un-rolled samples seen in Figure 3.20 and 3.21.

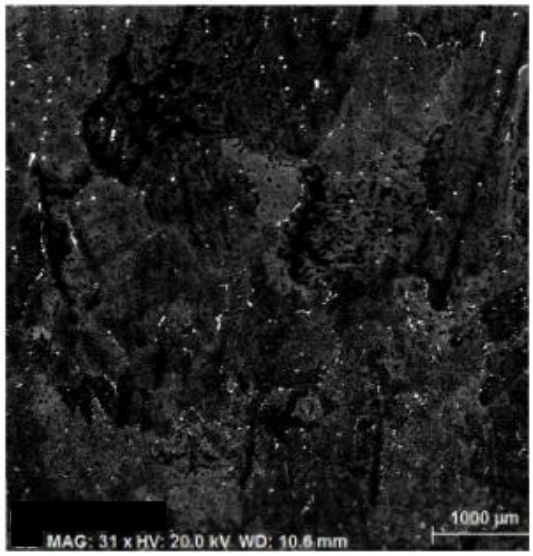

Figure 3.18: BSE image of sample induction heat treated for 20 min, cold rolled to 20.5 % reduction in thickness, and induction heat treated for 10 min.

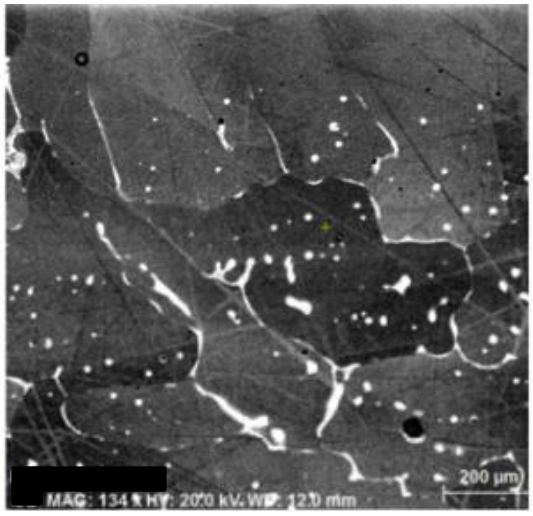

Figure 3.19: BSE image of 20 minute induction heat treatment, 20.5 % cold rolled reduction in thickness, 20 minute induction heat treatment. Note this sample is very edge material, and therefore received the least heat.

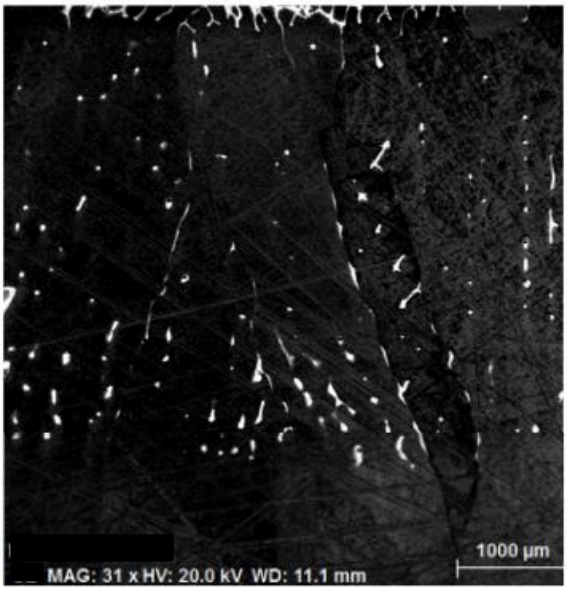

Figure 3.20: BSE image of 30 minute induction heat treatment.

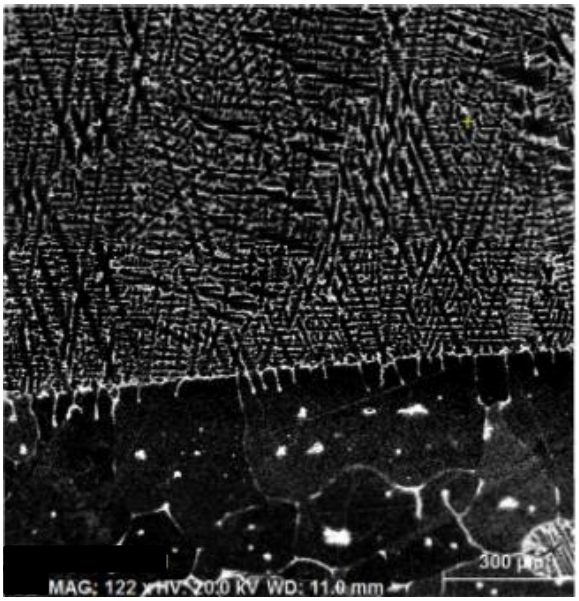

Figure 3.21: BSE Image of dendrite region still left in flipped, 40 minute induction heat treated sample.

Figure 3.21 reveals an important consideration with the induction heat treatments. By necessity, the sample sits on a copper plate within the induction coil. This bottom region of the sample therefore does not reach the same temperature as the entire sample. There is a clear boundary between the portion of the sample hot enough

to dissipate the tantalum, and that not, seen in the distinction between the top region with the tantalum (white) on the dendrite boundaries, and the lower region with it mostly dispersed. This region can be seen at the top of Figure 3.20 as well. To solve this problem, the samples must be flipped in the induction heat treatment so all regions spend sufficient time at the correct temperature to diffuse the tantalum uniformly in the bulk.

Table 3.6 illustrates another important feature of the additional heat treatment time, demonstrating that no longer is the grain boundary phase enriched with tantalum and aluminum, but simply tantalum. This intuitively makes sense, as tantalum is the larger, slower element with a much higher melting temperature, so the aluminum is quickly solutionized. (Ta normally 2.5 at%, Al 11.5 at%)

Table 3.6: Composition of boundary phase in cold rolled samples after 30 minute induction heat treatment.

El	AN	Series	unn. C [wt.%]	norm. C [wt.%]	Atom. C [at.%]	Error (1 Sigma) [wt.%]
Fe	26	K-series	33.20	36.79	39.85	0.91
Ni	28	K-series	23.28	25.80	26.58	0.65
Co	27	K-series	15.72	17.42	17.88	0.45
Al	13	K-series	4.27	4.73	10.59	0.24
Ta	73	L-series	13.77	15.26	5.10	0.42
		Total:	90.24	100.00	100.00	

Although most of the phase has been solutionized, it is not yet complete. An additional 20 minute induction heat treatment was performed on both the cold rolled as well as un-rolled samples, with both hot rolled at 1250°C following the final heat treatment. Figures 3.22 and 3.23 show NCATB that has been heat treated at just below melting temperature in the induction melter for 1 hour without any subsequent hot rolling. The dendritic region from solidification is still present although greatly reduced in size, seen

in the bottom of both images, with the tantalum mostly dispersed in the top region (not in contact with the copper plate during the heat treatment). However, the samples which underwent the same heat treatment, but with a subsequent 30% reduction in thickness hot rolling, have all elements in much better solution, seen in Figures 3.24 and 3.25. The bulk areas have minimal enrichment as shown with only few regions of the distinct white phase, and the dendritic region in the bottom of the figures no longer exists in full form, but instead has been reduced to very fine dispersed pockets of the tantalum rich phase.

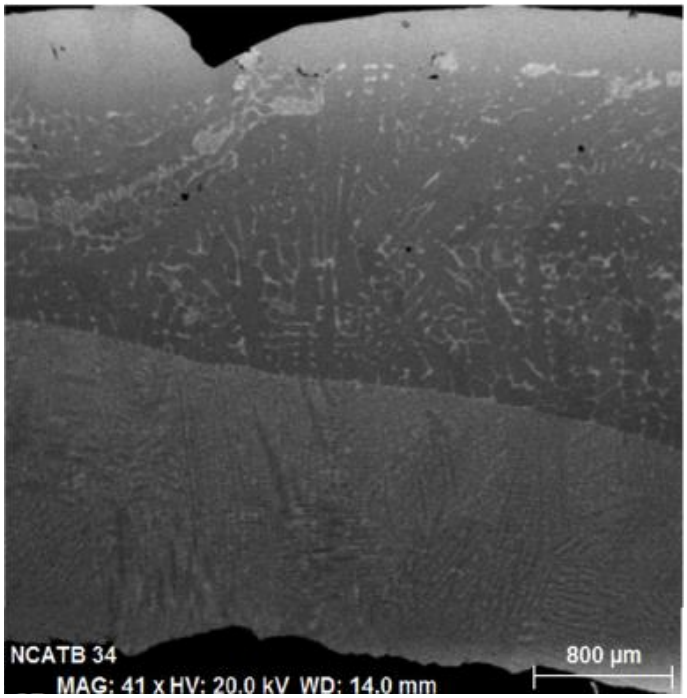

Figure 3.22: BSE image of 1 hour induction heat treated NCATB.

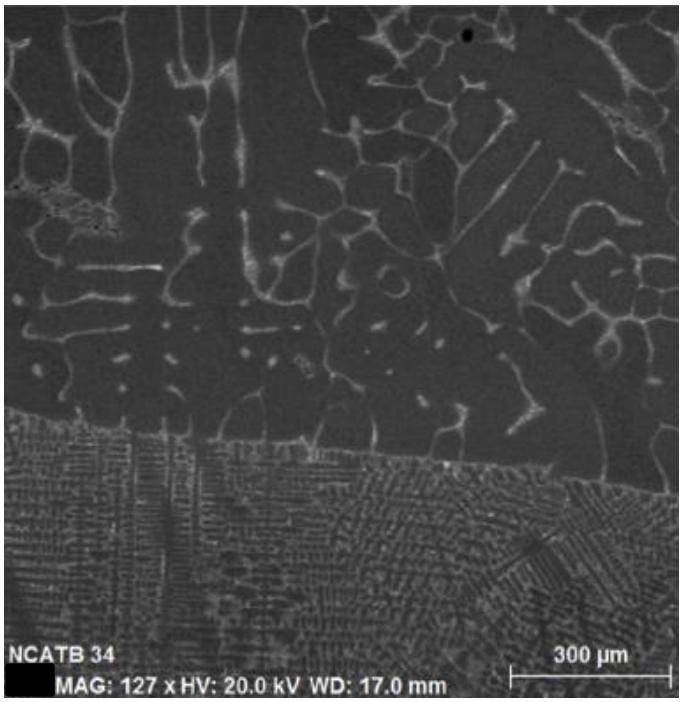

Figure 3.23: BSE image of 1 hour induction heat treated NCATB

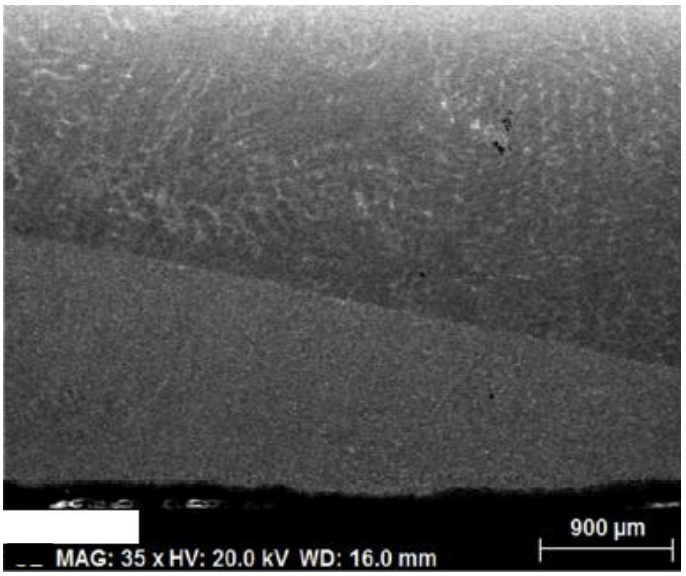

Figure 3.24: BSE image of 1 hour induction heat treated NCATB, followed by 30 % hot rolled reduction in thickness.

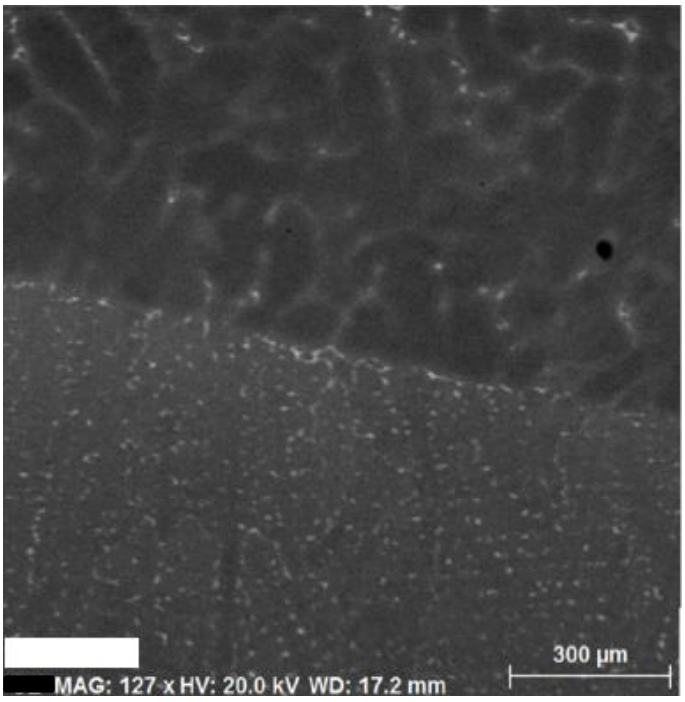

Figure 3.25: BSE image of 1 hour induction heat treated NCATB, followed by 30 % hot rolled reduction in thickness.

As expected, the NCATB with intermediate cold rolling to 20.5 % reduction in thickness following 20 minutes of high temperature induction heating, then another 40 minutes of induction treating following the rolling, with a final hot rolling step at 1250°C to 14 % reduction in thickness, had the best microstructure with nearly all elements in solution, including the tantalum, as seen in Figure 3.26. Additionally, Tables 3.7 and 3.8 show the composition of the white phase, and compared to the overall sample composition determined by EDS in Table 3.9, the boundary phase is only slightly richer in tantalum then the bulk, further minimization of the segregation. The tantalum composition in the boundary phase is 3.99 and 3.43 atom percent, compared to 3.18 atom percent in the full sample analyzed.

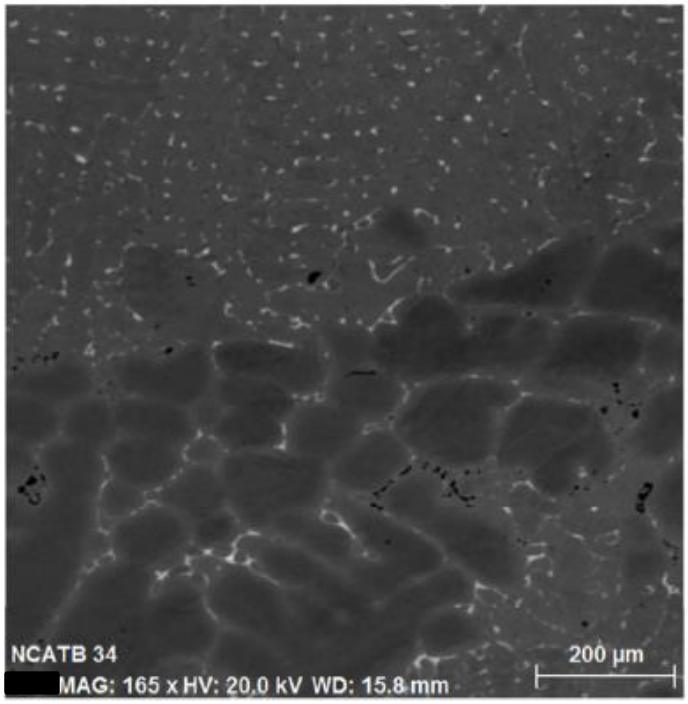

Figure 3.26: BSE image of NCATB induction heat treated 20 minutes, cold rolled, induction heat treated 40 minutes, and finally hot rolled.

Table 3.7: Composition of white boundary phase in cold and hot rolled NCATB seen in Figure 3.26, determined by EDS.

El	AN	Series	unn. C [wt.%]	norm. C [wt.%]	Atom. C [at.%]	Error (1 Sigma) [wt.%]
Fe	26	K-series	36.39	38.60	40.24	1.00
Ni	28	K-series	26.63	28.24	28.02	0.75
Co	27	K-series	16.33	17.32	17.11	0.48
Al	13	K-series	4.89	5.19	11.19	0.27
Ta	73	L-series	10.05	10.66	3.43	0.34
		Total:	94.29	100.00	100.00	

Table 3.8: Composition of second location of white boundary phase in cold and hot rolled NCATB seen in Figure 3.26, determined by EDS.

El	AN	Series	unn. C [wt.%]	norm. C [wt.%]	Atom. C [at.%]	Error (1 Sigma) [wt.%]
Fe	26	K-series	34.73	36.15	38.07	0.96
Ni	28	K-series	27.57	28.69	28.75	0.78
Co	27	K-series	16.80	17.49	17.45	0.49
Al	13	K-series	5.18	5.39	11.74	0.29
Ta	73	L-series	11.79	12.28	3.99	0.39
		Total:	96.06	100.00	100.00	

Table 3.9: Overall composition of entire NCATB sample cold and hot rolled seen in Figure 3.26, determined by EDS.

El	AN	Series	unn. C [wt.%]	norm. C [wt.%]	Atom. C [at.%]	Error (1 Sigma) [wt.%]
Fe	26	K-series	37.42	39.35	40.84	1.03
Ni	28	K-series	26.61	27.98	27.63	0.75
Co	27	K-series	16.76	17.62	17.33	0.49
Al	13	K-series	4.88	5.13	11.02	0.27
Ta	73	L-series	9.43	9.92	3.18	0.32
		Total:	95.10	100.00	100.00	

For reference, the overall composition desired in this alloy as reported by Tanaka [2] is Fe-28Ni-17Co-11.5Al-2.5Ta-0.05B. This composition is maintained in the entire bulk ingot, although the specific region of this sample, which is a worst-case edge material, has slightly more tantalum overall.

These inquiries into the methodology to obtain a homogenous sample with all elements in solution demonstrated that the combination of work, in the form of rolling, with the induction heat treatment, to a high degree uniformly disperse the tantalum. Additional ingots were arc and induction melted, and utilized the lessons learned from these studies on the tantalum dispersion to hopefully obtain complete solutionization. Specifically employed was the need for flipping the sample in the induction heat treatment for uniform heating, as well as an intermediate cold rolling step, and fine temperature control to ensure the sample does not re-melt in any of the heat treatments. Re-melting is a possible cause for the dendritic phase appearing in extended induction heat treatments, where reducing the sample size at the same power settings could have led to melting and therefore solidification. This was a challenge with removing material after each heat treatment step for SEM analysis, as the power setting for the previous sample size was not necessarily correct for the subsequent one. However, removing

material also meant that the sample remaining was pushed further towards edge material that would not have heated up as much as the bulk by the nature of the induction heating, as well as being cooler due to contact with the copper crucible. Therefore it cannot be concluded which of these two possibilities occurred, where it is likely that the dendrite region was an artifact of less heating. Visual inspection during the heat treatments did not reveal melting or shape change in the sample that would indicate liquidity and therefore melting. Since the remaining ingots would not have any material loss during the boundary phase dispersion, this problem would not be as strong, as the correct power setting was known and remained consistent at each step.

To obtain a uniform, fully solutionized NCATB alloy without any embrittling boundary phase, the ingots were induction heat treated just below melting temperature for 15 minutes, induction forged with rapid cooling, flipped, induction heat treated at the same temperature an additional 15 minutes, induction forged, hot rolled to 20 % reduction in thickness, induction heat treated 15 minutes, induction forged, flipped, induction heat treated a final 15 minutes, and induction forged with rapid cooling. Subsequently these ingots were hot rolled to 10 % reduction in thickness at 1250°C to minimize cracking, which developed in the previous samples, and to obtain the strong dispersion seen with the hot rolling step with the SEM BSE and EDS analyzed samples. An additional hot rolling step to 10 % reduction in thickness at 1250°C was added after the final 15 minute induction heat treatment to further break up the dendritic microstructure that may remain. These two samples were then solutionized for 10 hours at 1300°C in the Lindberg tube furnace under argon, on an alumina plate, as had been

performed with all other previous samples.

The hot rolled samples were cooled from 1300°C to room temperature in the Lindberg furnace, to minimize oxidation. This lead to the samples spending significant time, on the order of hours, at aging temperatures in the cooling process, with the samples having a HRB of 100 following the solutionization, indicating high levels of precipitation. A sample in this condition lacked the needed ductility for cold rolling, so to perfect this process and obtain fully solutionized NCATB, the samples were water quenched from 1300°C. The cost is slightly higher levels of oxidation, which is mechanically removed, but without any precipitation resulting at this step. The quenched NCATB had no problems rolling. Therefore the new processing is as follows:

1. Arc melting
2. Induction melting with rapid cooling induction forging
3. 15 minute high temperature heat treatment in induction melter, forged
4. Sample flipped in induction melter
5. 15 minute induction heat treatment, forged
6. 20 % hot rolled reduction in thickness at 1250°C
7. 15 minute induction heat treatment, forged
8. Flipped
9. 15 minute induction heat treatment, forged
10. 10 % hot rolled reduction in thickness
11. 10 hour 1300°C solutionization, water quenched
12. Cold rolling, recrystallization and aging

3.2.4: Superelastic Property

Now that the NCATB processing had been refined to completely eliminate the tantalum segregation along the grain boundaries, the cold rolled recrystallization would likely occur more rapidly and at lower temperatures, as there was no longer a phase pinning grain boundaries and slowing the transformation. 70 % reduction in thickness cold rolled samples that had been fully solutionized as reported in the previous section

were recrystallized at 1000°C for 2.5 minutes, 5 minutes, and 10 minutes, and water quenched. These samples were prepared for LOM analysis, including Nital etching. The microstructures revealed that 2.5 minutes at 1000°C did not recrystallize the NCATB, where recrystallization was beginning at 5 minutes, and nearly complete with very fine grains at 10 minutes, seen in Figure 3.27. To guarantee complete homogenous recrystallization, cold rolled samples were heat treated for 13 minutes.

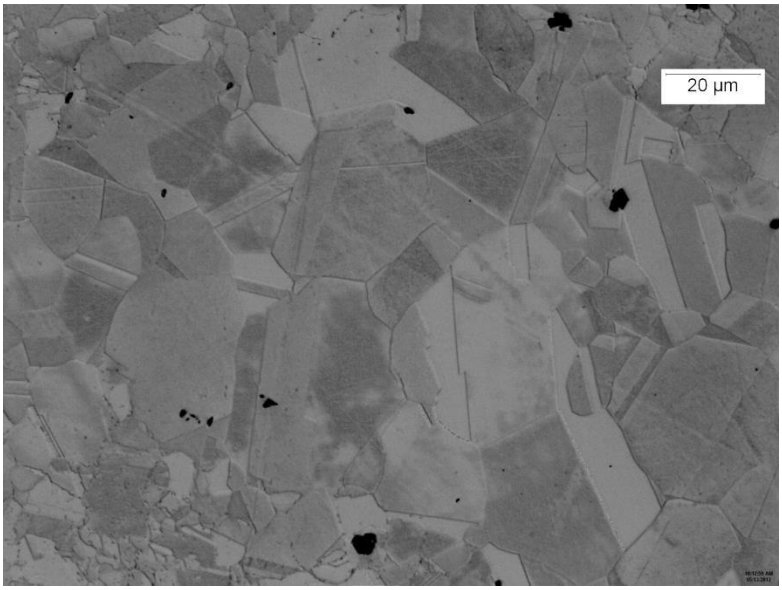

Figure 3.27: Micrograph of recrystallized NCATB, 1000°C for 10 minutes

The previous work on the hardening of the NCATB needed to be checked with these fully solutionized samples, as the reported processing by Tanaka [2] that results in no tantalum segregation, but large grains, did not achieve nearly as high hardness as fine grained NCATB with the detrimental enrichment. Therefore samples solutionized with the initial thermomechanical processing, cold rolled to 70% reduction in thickness, recrystallized at 1000°C for 13 minutes, and aged at 600°C were checked for hardness during the aging process. Seen in Graph 3.9, the refined processing is a further

improvement on the processing reported and utilized by Tanaka [2], and leads to better hardening than the 1300°C for 1 minute recrystallization series that still possessed the tantalum grain boundary segregation.

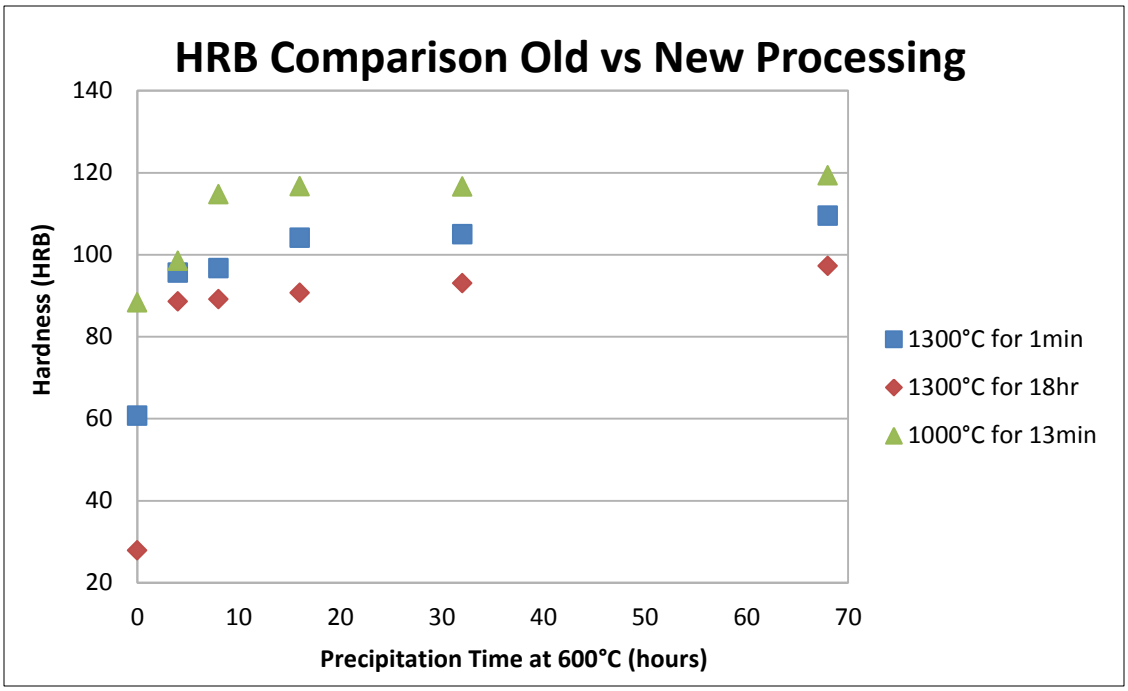

Graph 3.9: Hardness data including sample from refined high temperature thermomechanical processing before cold rolling.

Solutionizing the tantalum removes a phase pinning the grain boundaries and slowing the transformation, so it is intuitive that this series hardens quicker and to higher levels. By 8 hours at 600°C, the fine grained solutionized samples reach a Rockwell B hardness of 115, and by 16 hours achieve 117 HRB, the same hardness as the fine grained sample with the tantalum segregate aged for 213 hour at 600°C. Both are 54 HRC hardness. From 8 hours at 600°C to 68 hours at 600°C, the fine grained solutionized samples only harden from 115 HRB to 119 HRB, although these are near the maximum of the B hardness scale. Measured with the Rockwell C scale, this is an

increase from 49 HRC to 57 HRC, demonstrating that this in fact is further hardening. Graph 3.10 displays these measurements visually.

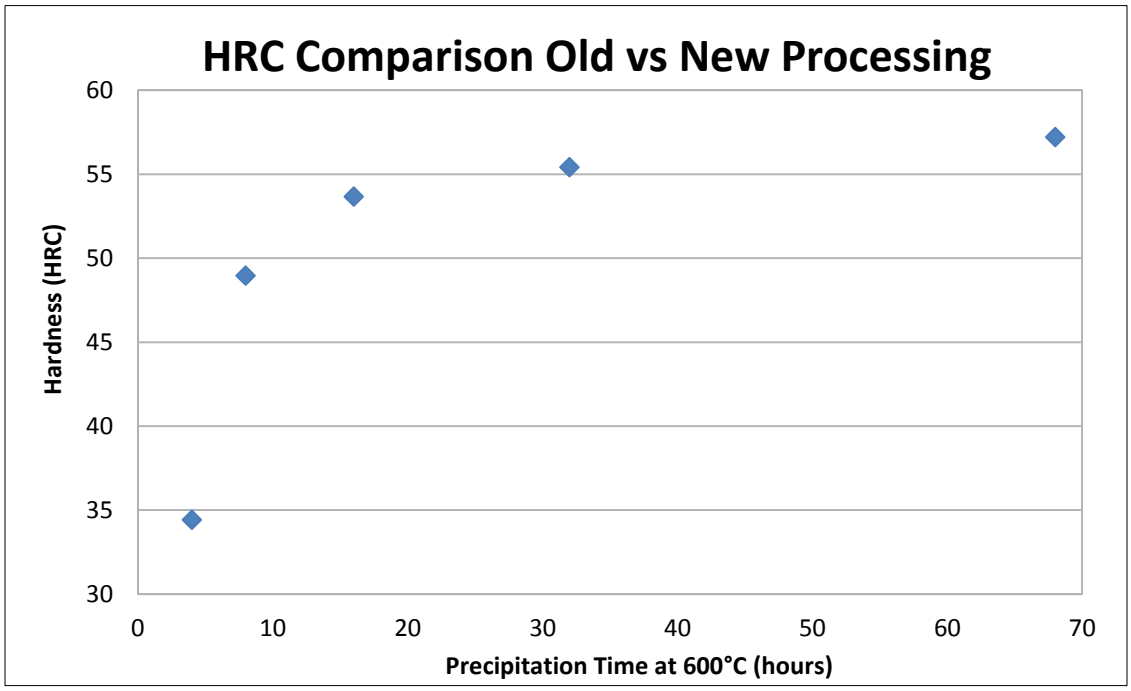

Graph 3.10: Hardness of fine grained solutionized NCATB measured with Rockwell C.

The values achieved with the full alloy solution, when compared to the hardness of NCATB with grain boundary tantalum, indicate that perhaps the presence of the segregate, while embrittling, in regards to hardenability acts more as a slowing agent in the kinetics of the precipitation, since extended times at 600°C for the NCATB with the segregate have nearly as high hardness as the fine grained, in complete solution, NCATB. Both Graphs 3.9 and 3.10 show that increased aging time does further harden the alloy, but it appears to have plateaued by 16 hours. Coupled with XRD analysis not showing a different segregate phase in the NCATB, as well as secondary electron imaging on the SEM not indicating a tantalum boundary crystallographic difference, the hardness data for the fine grained, fully solutionized NCATB confirms the previous

hardenability studies. The main difference is likely that all the hardness values would be increased by about 10 on the Rockwell B scale, had they been evaluated using a fully solutionized, fine grained sample.

The final experimental step left was to determine the end superelastic properties of the NCATB with its refined processing. The problem of the tantalum segregate has been fully eliminated, and its existence is likely why Tanaka *et al.* [2] reportedly desired such large grains, minimizing grain boundary area per volume. Using the extended solutionization following cold rolling served to dissipate the tantalum as well as grow grains. With this detrimental phase eliminated before the rolling step, the NCATB could now utilize grain refinement in enhancing its superelastic potential. Figure 3.28 shows LOM micrographs of the fully solutionized, fine grain NCATB microstructructure as it develops through the aging process. The γ' can be seen to precipitate preferentially on the grain boundaries, likely leading to the embrittlement still present in the alloy even after the problem of the tantalum segregate had been solved.

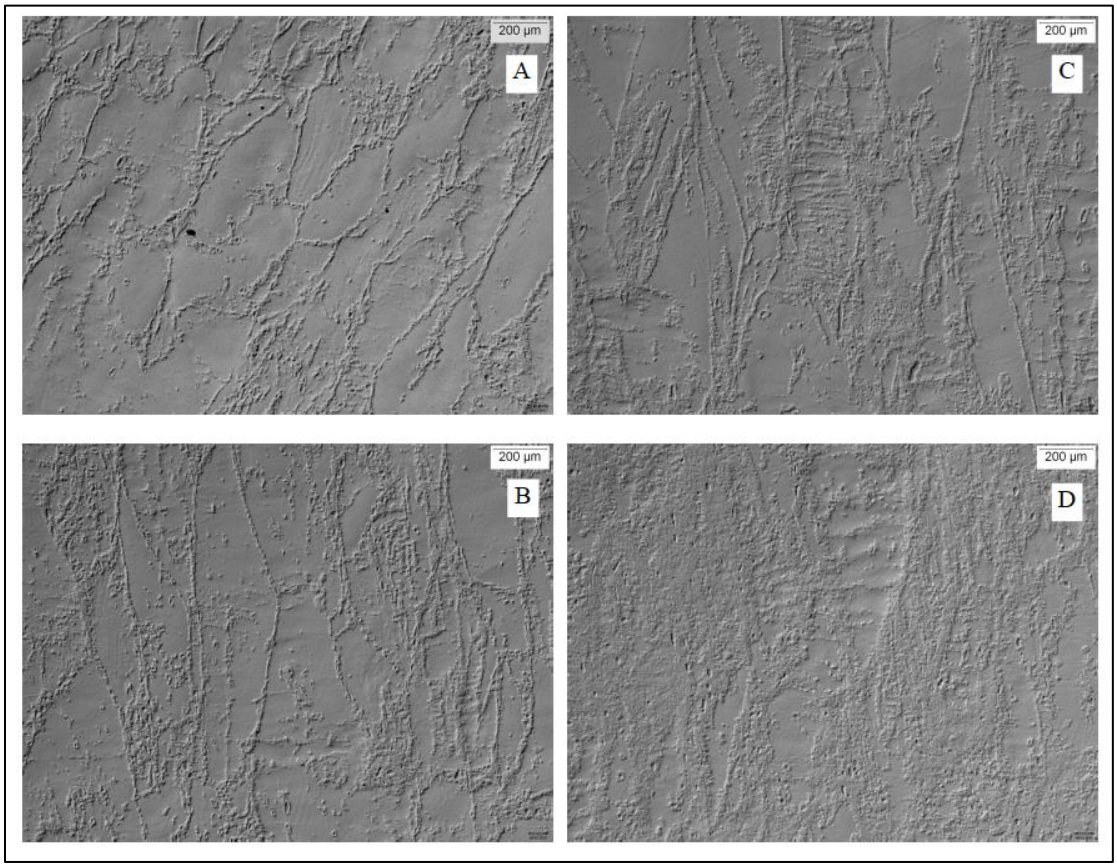

Figure 3.28: NCATB aged after refined processing at 600C for 8 hours (A), 16 hours (B), 32 hours (C), and 68 hours (D).

To check and ensure that this precipitate was not in fact the detrimental β phase reported by Tanaka [2] XRD and EDS analysis was performed on the samples. Figure 3.29 shows the XRD spectrum for the NCATB corresponding to the conditions in Figure 3.28, and there are no new phases, just the expected α' and γ/γ'. EDS taken of the precipitate also reveals an unchanged composition from the matrix, further proof that this is the γ' precipitate embedded in the γ austenite matrix, and not an entirely different precipitate.

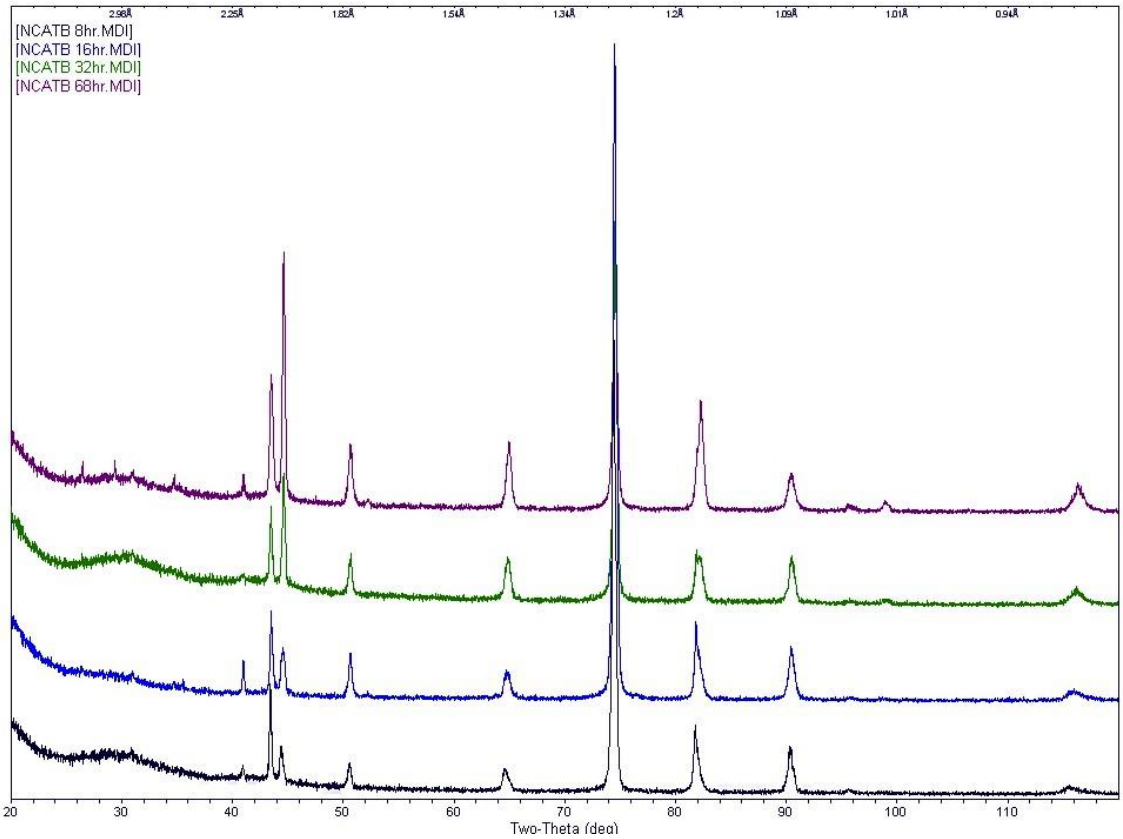

Figure 3.29: XRD spectrum of NCATB aged post process refinement

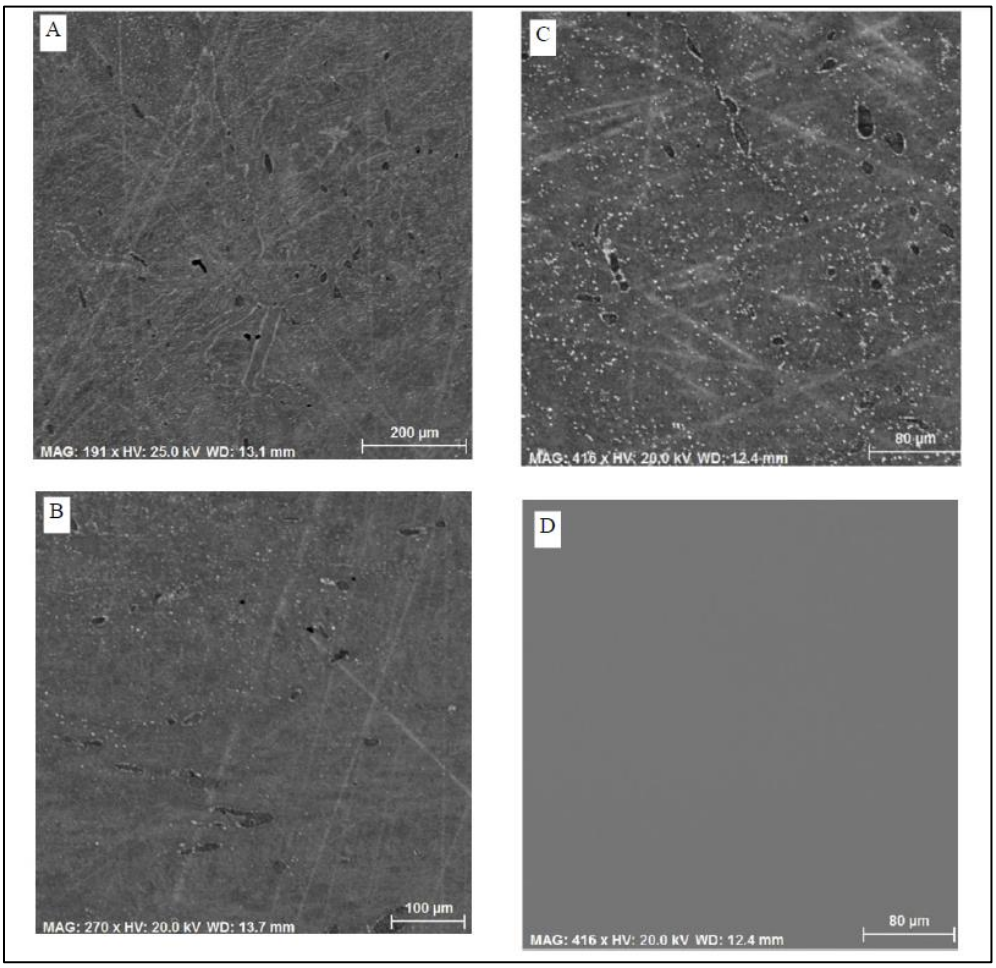

Figure 3.30: BSE image of NCATB aged post process refinement at 8 hours (A), 32 hours (B) and 68 hours (C), with secondary electron image at 68 hours (D)

Extensive EDS analysis of the entire BSE images revealed no new phases, just expected compositional variation, confirming the XRD data. Therefore, the precipitates seen in Figure 3.28 are conclusively γ'. The dark grains seen in the BSE images are almost always the normal elemental NCATB composition, although occasionally have aluminum variation, either increasing to 18 to 20 atom percent, coming at the exclusive cost of iron, or decreasing to 8 to 9 atom percent, again enriching the iron in the area.

These final studies have importantly revealed that although large strides have been made in developing the superelastic properties of NCATB, there is still much work left to be done. It is possible that the NCATB fully aged after the refined processing would exhibit superelatic properties. The refined processing distinctly improves the hardening properties of the alloy, and therefore hopefully strengthens the austenite matrix, enhancing the SE and SME. However, the precipitation of γ' does not seem to be coherent, as it nucleates preferentially on the recrystallized grain boundaries. Future work needs to be completed on fully evaluating the precipitation behavior as well as recrystallization time and temperature effect in fine grained NCATB that has utilized the refined processing determined in this work. These studies will hopefully make strides in eliminating the remaining embrittlement issues in the NCATB, allowing its full potential as a superelastic and shape memory alloy to be realized. This is a crucial step, as other iron based SMAs experience significant embrittlement that limits their superelasticity outside the single crystal state and therefore their commercial application. An attracting property of NCATB is its ductility, and while it already exhibits a good degree of ductility in rolling and post aging, there are still factors preventing the realization of its full ductility.

This chapter is currently being prepared for submission for publication of the material. Olson, Scott; Vecchio, Kenneth S. The thesis author was the primary investigator and author of this material.

CHAPTER 4: CONCLUSIONS

The detailed study of a new ferrous based alloy (Fe-28Ni-17Co-11.5Al-2.5Ta-0.05B at%) revealed that process improvement using lessons learned in developing Nitinol and other shape memory alloys enhanced the achieved properties and viability of this alloy. Specifically the introduction of a high temperature thermomechanical treatment before cold rolling eliminates the tantalum segregation that resulted in the dendritic microstructure from melting solidification. The addition of this processing removed the need for intermediate solutionization, and permitted fine grained NCATB to be aged to 119 Rockwell B hardness, 57 HRC. Even with the tantalum segregation on the grain boundaries, NCATB with a 10 μm average grain size resulting from a 1 minute recrystallization at 1300°C had markedly better hardening, by 12 HRB, compared to 18 hour recrystallized samples following the reported processing by Tanaka [2]. These samples with the tantalum segregation also revealed that any grain size control was still beneficial in aged hardness compared to large grains with full elemental homogenization.

Studies of other aging paths revealed that no precipitate variants form, only the known γ', where 600°C, 700°C and 800°C aged samples have equivalent hardness values at extended times, although the 700°C and 800°C temperatures harden the NCATB more quickly. 400°C and 500°C aging temperatures appear to be too slow kinetically to obtain the desired precipitation behavior, although at long times do harden to the levels of 18 hour large grained samples, which have the same hardness as fine grained samples with tantalum segregation after 4 hours at 600°C.

Specifically the research of this thesis revealed:

1. A 1300°C for 0.5 minute heat treatment in a Ta-segregate sample recrystallized to 11 μm grain size and 105 HRB after 68 hour aging at 600°C.
2. A 1300°C for 1 minute heat treatment in a Ta-segregate sample recrystallized to 10 μm grain size and 109 HRB after 68 hour aging at 600°C, and 117 HRB or 54 HRC after 213 hours at this temperature.
3. A 1300°C for 1.5 minutes heat treatment in a Ta-segregate sample recrystallized to 51 μm grain size and 108 HRB after 68 hour aging at 600°C.
4. A 1300°C for 2 minutes heat treatment in a Ta-segregate sample recrystallized to 80 μm grain size and 105 HRB after 68 hour aging at 600°C.
5. A 1300°C for 2.5 minutes heat treatment in a Ta-segregate sample recrystallized to 107 μm grain size and 106 HRB after 68 hour aging at 600°C.
6. A 1300°C for 3 minutes heat treatment in a Ta-segregate sample recrystallized to 124 μm grain size and 97 HRB after 68 hour aging at 600°C.
7. The processing as reported by Tanaka *et al.* [2] results in a 400 μm grain size and 97 HRB fully aged.
8. A 1150°C for 12 minutes heat treatment in a Ta-segregate sample recrystallized to 5 μm grain size and 102 HRB after 68 hour aging at 600°C.
9. A 1225°C for 2 minutes heat treatment in a Ta-segregate sample recrystallized to 35 μm grain size and 106 HRB after 64 hour aging at 600°C.
10. A 1225°C for 10 minutes heat treatment in a Ta-segregate sample recrystallized to 102 μm grain size.

11. A 1300°C for 1 minute heat treatment in a Ta-segregate achieved 91 HRB after 68 hour aging at 400°C, 93 HRB after 128 hours, and 90 HRB after 672 hours at this temperature.
12. A 1300°C for 1 minute heat treatment in a Ta-segregate achieved 94 HRB after 128 hour aging at 500°C, and 99 HRB after 672 hours at this temperature.
13. A 1300°C for 1 minute heat treatment in a Ta-segregate achieved 105 HRB after 32 hour aging at 700°C, and 109 HRB after 48 hours at this temperature.
14. A 1300°C for 1 minute heat treatment in a Ta-segregate achieved 107 HRB after 8 and 16 hour aging at 800°C.
15. Thermomechanical processing prior to cold rolling eliminates the Ta-segregate and allows a 10 μm recrystallized grain after 13 minutes at 1000°C, aged at 600°C for 16 hours to achieve 117 HRB or 54 HRC, and after 68 hours 119 HRB or 57 HRC.
16. XRD analysis did not reveal any precipitant variant in aging paths from 400ºC to 800ºC.

This chapter is currently being prepared for submission for publication of the material. Olson, Scott M.; Vecchio, Kenneth S. The thesis author was the primary investigator and author of this material.

APPENDIX

Appendix A: Reported Processing Microstructural Evolution

To determine the best original research that could be contributed on this ferrous shape memory alloy, it was first necessary to understand the microstructural development of the NCATB alloy through its reported processing steps. Therefore the alloy was arc and induction melted, hot rolled at 1250°C to 28 % reduction in thickness, solutionized at 1300°C for 15 minutes, cold rolled at room temperature to 98 % reduction in thickness, solutionized at 1300°C for 18 hours, and aged at 600°C for 72 hours, with samples taken for LOM and XRD analysis. Figures A.1 through A.4 summarize the findings.

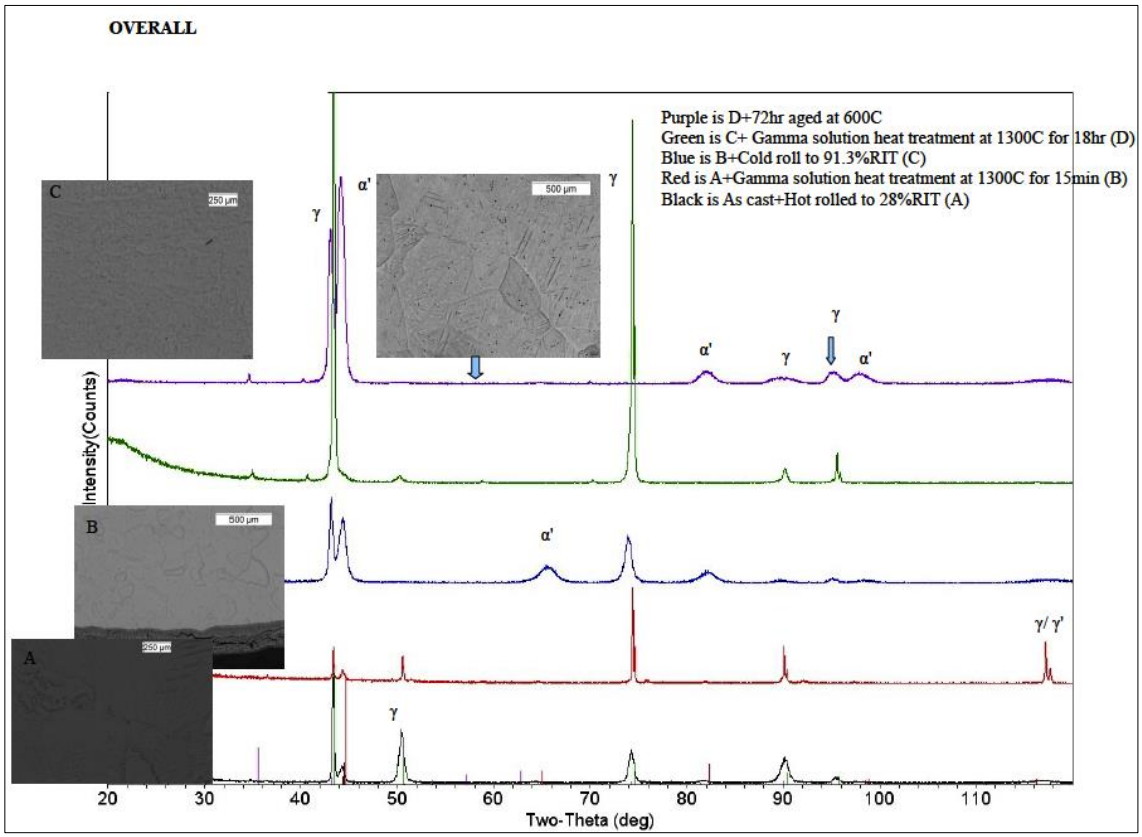

Figure A.1: Overall development of NCATB microstructure with reported processing.

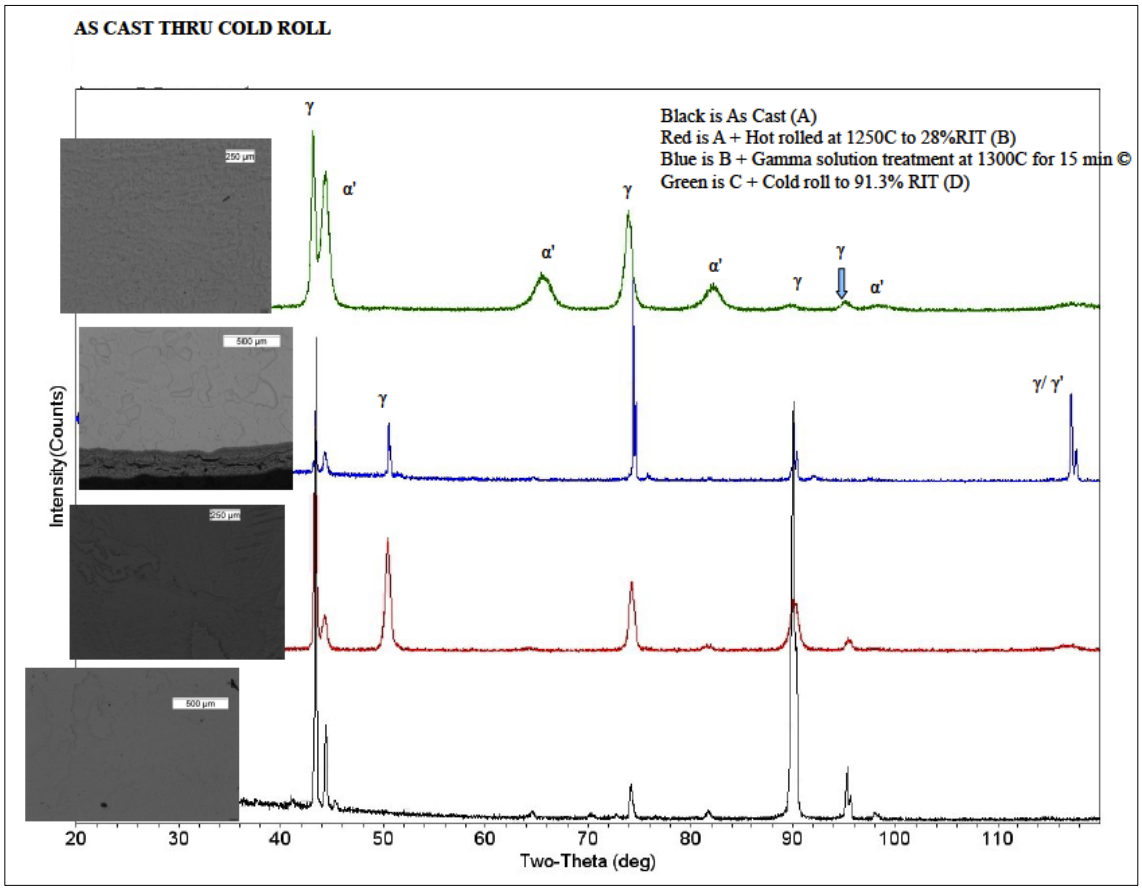

Figure A.2: Development of as cast through cold rolling of NCATB microstructure with reported processing.

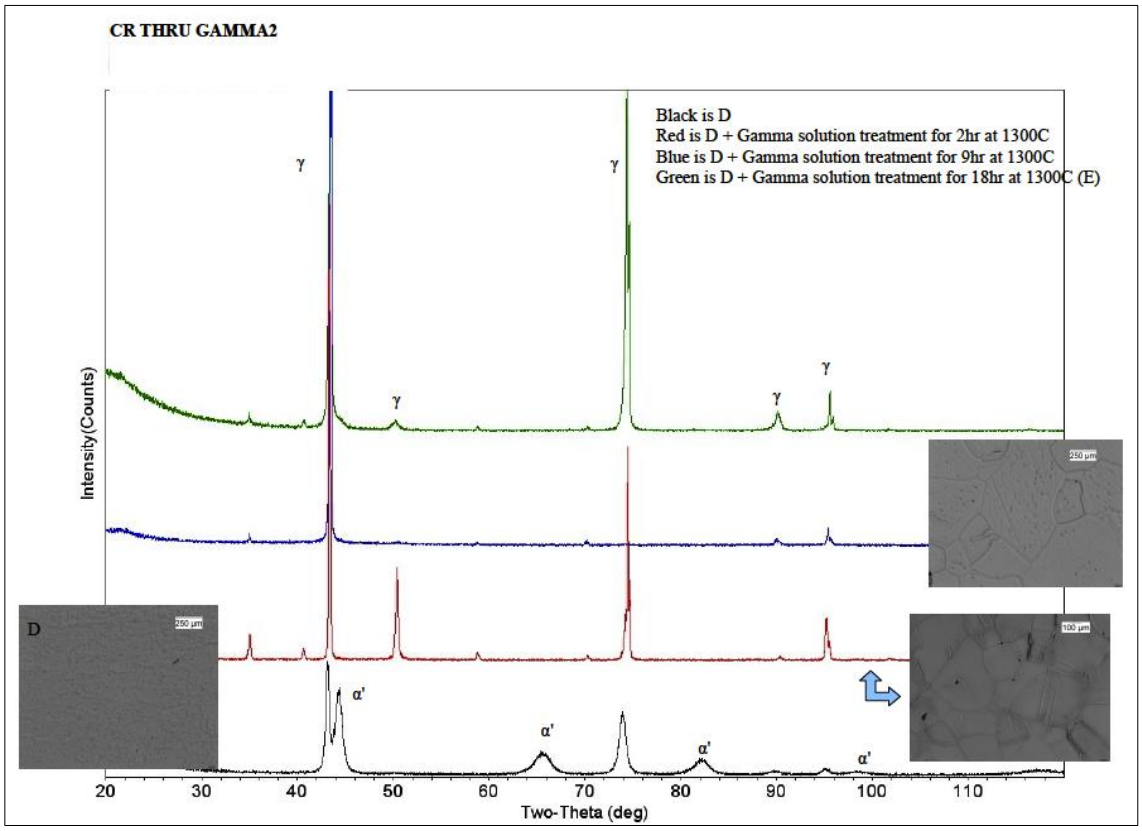

Figure A.3: Development of cold rolled through secondary solutionization of NCATB microstructure with reported processing.

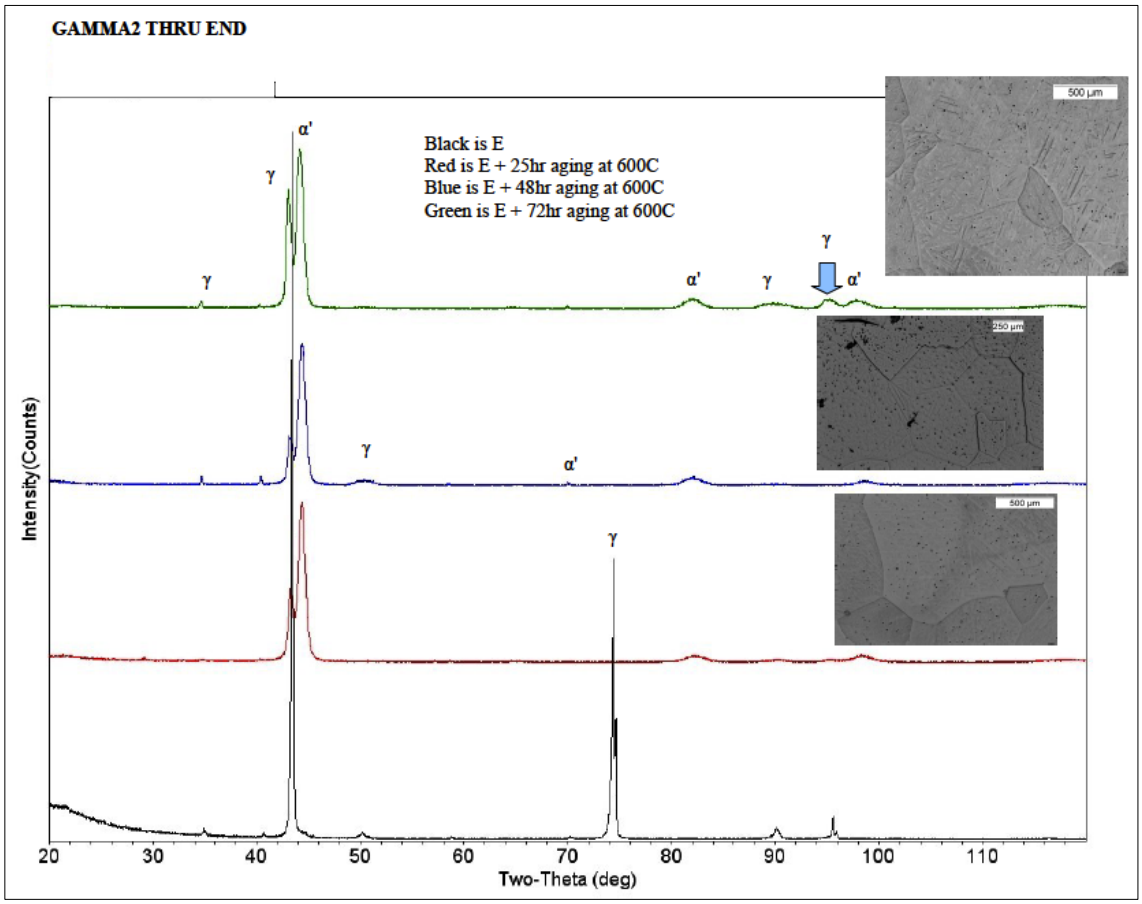

Figure A.4: Development of NCATB microstructure with reported processing from secondary solutionization through final aging.

The research on the microstructural development through the reported processing revealed the importance of strengthening the austenite γ matrix to allow for the formation of the stress induced martensite, as seen in the presence of the martensite lathes in the optical micrographs, as well as the presence of the α' peaks in the XRD spectrum. The solutionization and melting steps have no to minimal SIM and therefore do not have sufficient resistance to dislocation slip and plastic deformation in the austenite matrix, making the alloy lack superelastic or shape memory properties. Mechanical work as well as precipitation are both mechanisms that strengthen the γ phase by strain hardening the alloy with the rolling, and precipitation hardening it with

the aging treatment. These are common and well established strengthening paths in metals. Importantly, the SIM peaks appear in the XRD spectrum strongly for the cold rolled samples, as well as expectedly strengthen through the aging process. This highlights the importance of these two steps to developing the superelasticity, consistent with results from Tanaka and Chumlyakov on NCATB, which guided the research reported in this thesis [2,21-29].

This chapter is currently being prepared for submission for publication of the material. Olson, Scott M.; Vecchio, Kenneth S. The thesis author was the primary investigator and author of this material.

REFERENCES

1. Dadda, Maier, Niklasch, Karaman, Karaca and Chumlyakov. Metall. And Mat. Trans A Vol. 39A (2008) pp 2026.
2. Tanaka, Himuro, Kainuma, Sutou, Omori, and Ishida. Science Vol. 327 (2010) pp 1488.
3. Otsuka and Wayman, Shape Memory Materials. Cambridge University Press. ISBN 0 521 44487 X.
4. Kajiwara, Baruj, Kikuchi and Shinya. Proc. Of SPIE, Vol. 5053 pp 250
5. Cherenko, Kokorin, Vitenko and Bugaychuk. Journal de Physique IV, Colloque C8, Vol. 5 (1995) pp 481
6. Maki, Kobayashi, Minato and Tamura. Scripta METALLURGICA, Vol. 18 (1984) pp 1105-1109
7. Kajiwara and Kikuchi. Acta Matell. Mater. Vol 38, No 5. (1990) pp 847-855.
8. Dadda. Metall. And Mat. Trans A. Vol 39A (2008) pg 2026.
9. Kajiwara. Mat Sci and Eng A273-275 (1999) pp 67-88.
10. Grosdidier and Philippe. Mat Sci and Eng A291 (2000) pp 218-223.
11. Adharapurapu, Jiang, and Vecchio. Mat Sci and Eng A527 (2010) pp 1665-1676.
12. Huang and Liu. Scripta Materialia 45 (2001) pp 153-160.
13. Maeshima, Ushimaru, Yamauchi and Nishida. Mat Sci and Eng A438-440 (2006) pp 844-847.
14. Sutou, Koeda, Omori, Kainuma and Ishida. Acta Materialia 57 (2009) pp 5759-5770.
15. Sutou, Omori, Kainuma, Ono and Ishida. Metallurgical and Mat Trans. A 33A (2002) pp 2817-2824.
16. Baruj, Kikuchi, Kajiwara and Shinya. Mat Sci and Eng A 378 (2004) pp 333-336.
17. Tanaka, Oikawa, Sutou, Omori, Kainuma and Ishida. Mat Sci and Eng A 438-440 (2006) pp 1054-1060.
18. Kim, Ikehara, Kim, Hosoda, and Miyazaki. Acta Materialia 54 (2006) pp 2419-2429.
19. Kireeva, Chumlyakov, Kirillov, Kretinina, Danil'son, Karaman, and Cesari. Russian Physics Journal, Vol 53, No 10 (2011).
20. Kireeva, Chumlyakov, Kirillov, Karaman and Cesari. Technical Physics Letters, Vol 47, No 5 (2001) pp 487-490.
21. Chumlyakov, Kireeva, Panchenko, Karaman, Maier, Timofeeva. J. Alloys Compd. (2012)

22. Ma, Kockar, Evirgen, Karaman, Luo, Chumlyakov. Acta Materialia 60 (2012) pp 2186-2195.

23. Ma, Hornbuckle, Karaman, Thompson, Luo, and Chumlyakov. Acta Materialia 61 (2013) pp 3445-3455.

24. Chumlyakov, Kireeva, Panchenko, Kirillov, Timofeeva, Kretinina, Danil'son, Karaman, Maier, and Cesari. Russian Physics Journal, Vol 54, No 8 (2012).

25. Chanda, Pal, De, Kajiwara and Kikuchi. Mat Sci and Eng A265 (1999) pp 110-116.

26. Monroe, Karaman, Karaca, Chumlyakov and Maier. Scripta Materialia 62 (2010) pp 368-371.

27. Sugiyama, Oshima, and Fujita. Trans. Of the Japan Inst. Of Metals, Vol 27, No 10 (1986) pp 719-730.

28. Miyazaki, Otsuka and Wayman. ISIJ International, Vol 29, No 5 (1989) pp 423-429.

29. Chumlyakov, Panchenko, Kireeva, Karaman, Sehitoglu, Maier, Tverdokhlebova, and Ovsyannikov. Mat Sci and Eng A 481-482 (2008) pp 95-100.

30. Geng, Jin, Ren, Zhang and Jin. J. Alloys Compd. (2012).